

Constraining new physics effective interactions via a global fit of electroweak, Drell-Yan, Higgs, top, and flavour observables

J. de Blas^a, A. Goncalves^b, V. Miralles^{c,d}, L. Reina^b, L. Silvestrini^e and M. Valli^e

^a*Departamento de Física Teórica y del Cosmos, Universidad de Granada, Campus de Fuentenueva, E-18071 Granada, Spain*

^b*Physics Department, Florida State University, Tallahassee, FL 32306-4350, USA*

^c*Departament de Física, Universitat d'Alacant, Campus de Sant Vicent del Raspeig, E-03690 Alacant, Spain*

^d*School of Physics and Astronomy, University of Manchester, Oxford Road, Manchester M13 9PL, UK*

^e*INFN, Sezione di Roma, Piazzale A. Moro 2, I-00185 Rome, Italy*

E-mail: deblas@ugr.es, agoncalvesdossantos@fsu.edu,
victor.miralles@ua.es, reina@hep.fsu.edu,
luca.silvestrini@roma1.infn.it, mauro.valli@roma1.infn.it

ABSTRACT: We present results from a global fit of Standard Model parameters and dimension-6 SMEFT Wilson coefficients that includes electroweak, Drell-Yan, Higgs-boson, top-quark, and flavour observables. Fits obtained by floating individual coefficients are also discussed. The leading-order scale dependence of the SMEFT Wilson coefficients is consistently included in the evolution from the UV scale to the electroweak scale and the low-energy scale of flavour observables. In defining the SMEFT set of active operators we consider both the $U(3)^5$ and the $U(2)^5$ flavour symmetric limits. All fits are obtained within the HEPfit framework and are based on the most recent experimental results and state-of-the-art theoretical predictions for all the observables considered.

Contents

1	Introduction	1
2	Framework: effective interactions from new physics	5
2.1	The Standard Model Effective Field Theory: formalism and assumptions	5
2.2	Renormalization group evolution in the SMEFT	7
3	Constraints on new physics from current data	8
3.1	Introduction to the fitting procedure	8
3.2	General setup for theoretical predictions	9
3.3	Electroweak and Drell-Yan observables	10
3.4	Higgs-boson observables	12
3.5	Top-quark observables	13
3.6	Flavour observables	14
3.6.1	$\Delta F = 2$ observables	14
3.6.2	$\Delta F = 1$ observables	16
4	Results	18
4.1	Results for the $U(3)^5$ flavour symmetric SMEFT	18
4.2	Results for the $U(2)^5$ flavour symmetric SMEFT	21
5	Conclusions	25
A	Relations between SMEFT operators under different flavour assumptions	31
A.1	$U(3)^5$ flavour symmetric SMEFT	31
A.2	$U(2)^5$ flavour symmetric SMEFT	31
B	Tables of results	33
B.1	Results for the $U(3)^5$ flavour symmetric SMEFT	33
B.2	Results for the $U(2)^5$ flavour symmetric SMEFT	35

1 Introduction

The consistency and predictivity of the Standard Model (SM) of particle physics up to energy scales of a few hundred GeV is impressive and has reached an unprecedented level of accuracy. At the same time its limits are well known: from missing a viable candidate of dark matter to not explaining the baryon asymmetry of the universe or the nature of dark energy. Furthermore, constituents of the SM itself, namely the Higgs boson and neutrinos, are still quite mysterious. Indeed, neutrino masses cannot be described within the SM and

require a new physics (NP) explanation. On the other hand, the properties of the Higgs boson as well as the origin of the electroweak (EW) symmetry breaking are encoded but not explained by the SM, and the Higgs particle could be a potential messenger of NP. Although weakly-interacting light NP may have escaped detection so far, most likely the explanation of these phenomena is to be sought at energies beyond the ones directly probed so far, in a still unknown *ultraviolet* (UV) theory that reduces to the SM at energy scales of a few hundred GeV.

Low-energy experiments as well as high-energy lepton and hadron colliders such as LEP, the Tevatron, past and present B-factories, and the Large Hadron Collider (LHC) have set lower bounds on UV physics beyond the SM (BSM) both directly and indirectly. Given the energies explored and the absence of deviations from SM predictions, often probed with percent or permille level sensitivity, we expect potential NP to live at energies quite above the EW scale, namely at or above the TeV scale. Indeed the region between 1-10 TeV will be the focus of the high-luminosity LHC (HL-LHC) and of future-collider explorations, both via higher precision and higher energy.

From a theoretical point of view, the problem of investigating the effects of unknown heavy NP lends itself naturally to an effective field theory (EFT) approach, where the effects of NP at the EW scale are encoded in non-renormalizable local interactions of the SM fields. The SM is then to be seen as the 4-dimensional part of a more general EFT whose Lagrangian also includes operators of higher dimension obtained from the projection of a given UV theory onto the space of fields of the SM. The SM Effective Field Theory (SMEFT) realizes this idea by extending the Lagrangian of the SM by a complete set of Lorentz and (SM-)gauge invariant effective interactions of increasing mass dimensionality, built in terms of SM fields. These interactions do, in general, break the SM accidental symmetries but could also satisfy additional discrete and global symmetry properties, depending on the kind of NP they encode (see [1, 2] for a general introduction and [3] for a state-of-the-art review of the SMEFT and its studies).

Different UV extensions of the SM project differently on the effective interactions of the SMEFT Lagrangian below the UV scale Λ [4–6], such that constraining the effect of SMEFT interactions with available data could discriminate between classes of UV models and guide future BSM explorations. Most notably, different flavour symmetries assumed at the UV scale Λ modify the number and structure of SMEFT interactions present below Λ and directly affect a broad spectrum of observables. Several studies [7–18] have investigated the impact of different UV flavour assumptions and emphasised the need to move beyond the initial flavour-blind approach. A popular first step beyond assuming complete invariance under family rotation for the five kinds of fermions present in the SM (the so-called $U(3)^5$ flavour symmetry of the two left-handed doublets and three right-handed singlets of the SM gauge group) consists in singling out the third generation and still assuming invariance under rotation within the first two families (the so-called $U(2)^5$ flavour symmetry assumption). This choice is motivated by the scale hierarchy present among fermions and naturally appears in several BSM models. In our study we will consider both cases and discuss pros and cons of both assumptions in current fits. We emphasize that when specifying the flavour symmetry we only refer to the NP contribution encoded in the

Wilson coefficients of operators of $d > 4$. Typical examples of such NP models are given by heavy gauge bosons coupling universally to all flavours ($U(3)^5$, see e.g. ref. [19]) or coupling differently to the third generation ($U(2)^5$). Since the $U(2)^5$ symmetry describes to a good approximation the quark flavour structure of the SM, one could also assume that the flavour invariance involves also the renormalizable part of the Lagrangian, with suitable breaking terms arising in both the $d \leq 4$ and $d > 4$ terms in the SMEFT, as discussed in detail in ref. [8] and typically happening in models seeking to explain the SM flavour hierarchy (see for example ref. [20]).

The EFT framework also allows to systematically account for quantum effects. In particular, the SMEFT Wilson coefficients satisfy well-defined renormalization group (RG) equations that allow to determine their scale dependence and evolve them from the UV scale Λ to the lower scales where they enter the calculation of physical observables. In this way, not only the precision of theoretical predictions of such observables is improved by a more efficient resummation of their perturbative expansion, but the potentially large interplay between different operators that mix under renormalization group evolution (RGE) is taken into account.

Overall, the great advantage of employing an effective field theory framework is that we can implement in a very general and systematic way a bottom-up approach to the exploration of some unknown UV theory using our knowledge of the physics we can currently test. Had patterns to emerge (e.g. enhanced or suppressed SMEFT coefficients, correlation and flat directions in SMEFT space, etc.) they could help in selecting classes of models whose investigation could then become more specific. The effective field theory framework is also useful in this regard. Using a top-down approach, one can easily re-interpret the SMEFT results in terms of specific models by using the matching between a given UV scenario and the effective theory. In the absence of unambiguous signs of BSM physics, the SMEFT general approach, although less informative, can indeed provide a very powerful exploratory tool. With this respect, we now have at our disposal for the first time a very broad spectrum of sufficiently accurate experimental measurements that can be simultaneously used to constrain the effective interactions of the SMEFT. This has indeed become a major effort in particle physics phenomenology and various comprehensive studies based on fits of the SMEFT that include a broad spectrum of observables have appeared in the recent literature [15, 16, 21–28].

In this paper we present the results of both individual and global fits of the SMEFT coefficients that include EW, Drell-Yan, Higgs-boson, top-quark, and flavour-physics observables. For the first time in the literature, in each fit we also float all SM parameters and all the relevant hadronic parameters in the flavour sector, thus taking fully into account the SM parametric and theoretical uncertainties, which are mostly relevant in the flavour sector. This turns the global fit into a highly challenging endeavour, particularly for the $U(2)^5$ case where it involves a total of about two hundred parameters.

We will be working in the SMEFT between the UV scale Λ and the EW scale (μ_W), while at μ_W we will transition to the Low Energy Effective Theory (LEFT) [29] where all the heavy SM degrees of freedom (W, Z, H, t) are integrated out. To fully benefit of the EFT formalism and in order to account for impactful quantum effects, we will consider

the scale dependence of the SMEFT and LEFT Wilson coefficients using leading-order RGE, with tree-level matching conditions at the EW scale μ_W . All fits are performed in the open-source `HEPfit` framework [30, 31] using for each observable state-of-the-art theoretical predictions and the most recent experimental measurements.

The outcome of the fits presented in this paper will determine the ranges of SM parameters and SMEFT Wilson coefficients at the UV scale Λ that are compatible with the selected broad set of experimental measurements. We will present both fits in which only one coefficient at a time is active and fits in which all SMEFT coefficients are simultaneously active at the scale Λ . Single-coefficient fits can be used to extract information on the set of observables that most constrain a given coefficient and can also give preliminary indications on the main RGE effects, while the global fit fully represents the combined effect of using a broad spectrum of observables and considering the operator mixing induced by the RGE. At the same time, a global fit of SM parameters and SMEFT coefficients can be very sensitive to the parametric and theoretical uncertainties and thus less effective, given current accuracies, to constrain the theory at hand. This dilution of the sensitivity is less evident in the $U(3)^5$ scenario, but has a strong impact in the $U(2)^5$ case, calling for the inclusion of more observables and/or for higher theoretical and experimental precision on the currently included ones.

Furthermore, in order to determine to which extent with current data we can constrain NP living at different scales, we will consider two representative benchmark values for the NP scale: $\Lambda = 3$, and 10 TeV including full RGE, and also compare them with results obtained without RGE (and $\Lambda = 1$ TeV). Not knowing the scale of NP, this is quite relevant to answer the fundamental question about what kind of observables are going to play the most important role and to what level of precision we need to determine them both theoretically and experimentally in order to explore NP up to a scale of 10 TeV.

The paper consists of this introductory section followed by three main core sections and two appendices. A final section summarises the main conclusions of our study and presents an outlook on future developments. Concerning the core sections, in Section 2 we review elements of the SMEFT relevant to our study with particular emphasis on the implementation of the two aforementioned flavour scenarios, namely $U(3)^5$ and $U(2)^2$, and a detailed discussion of how the RGE of the SMEFT coefficients and SM parameters is included in our study. Technical details on how these two scenarios are implemented in the SMEFT basis of operators considered in our study are provided in Appendix A. Section 3 is dedicated to a discussion of the fitting framework and procedure, including how the various sets of observables have been implemented in `HEPfit`. A complete set of results is illustrated and discussed in Section 4 while the full outcome of both individual and global fits, for all three UV scales $\Lambda = 1, 3$, and 10 TeV, with and without RGE, are collected in a series of tables in Appendix B.

2 Framework: effective interactions from new physics

2.1 The Standard Model Effective Field Theory: formalism and assumptions

Assuming the presence of a significant mass gap between the scale of NP Λ and the energies explored in current experiments, we can describe NP effects via the SMEFT Lagrangian:

$$\mathcal{L}_{\text{SMEFT}} = \mathcal{L}_{\text{SM}} + \sum_{d>4} \frac{1}{\Lambda^{d-4}} \sum_i C_i^{(d)} \mathcal{O}_i^{(d)}, \quad (2.1)$$

where $\mathcal{O}_i^{(d)}$ are Lorentz and (SM)-gauge invariant operators of canonical mass dimension d built only of SM fields, i collectively labels each operator according to its field composition and quantum numbers, and Λ is the cutoff of the effective theory indicatively identified with the UV scale of NP. If lepton number is conserved by the NP, the leading-order effects appear at dimension 6. In this work, we truncate the $\mathcal{L}_{\text{SMEFT}}$ to include only dimension-6 operators and adopt the Warsaw basis introduced in ref. [32]. We also neglect baryon number violating and CP-odd operators. This results in the set of operators listed in Table 1.

Furthermore, we do not consider the operator \mathcal{O}_ϕ since it does not enter at leading order in any of the observables considered in this study. In fact, the main effect of this operator is to modify the Higgs-boson self-interactions, and can only be weakly constrained with current Higgs pair-production data [33, 34]. We also notice that while this operator can be generated from other bosonic interactions via renormalization (to be discussed in Section 2.2), it does not enter in the 1-loop anomalous dimension matrix entries for any other SMEFT interaction, i.e. no other operator is generated from a non-zero value of C_ϕ at the UV scale.

In this study we consider two possible flavour assumptions at the new-physics scale: the $U(3)^5$ and the $U(2)^5$ flavour symmetric limits. The $U(3)^5$ limit assumes that the NP is flavour-blind, and leaves a total of 41 independent Wilson coefficients (40 if not considering C_ϕ). The notation for these coefficients and the relations with the SMEFT Wilson coefficients in the general case are presented in Appendix A.1.

To define the $U(2)^5$ limit, it is necessary to specify a direction in flavour space that identifies the third generation. In this work, we choose the direction of the third family to be the one defined by the Yukawa couplings at the NP scale Λ , and consider the two possibilities where the third family is defined: 1) in the basis of diagonal up-type quark Yukawa couplings (denoted as *UP basis* in the following), or 2) in the basis of diagonal down-type quark Yukawa couplings (denoted as *DOWN basis* in the following). It is important to emphasise that these two classes of scenarios do not correspond to a mere change of basis, but rather reflect different assumptions about the flavour structure of the underlying UV physics. Notice that such a flavour misalignment arises exclusively in the left-handed quark sector — see the discussion in [35] — while right-handed quark Yukawa couplings, as well as the full charged-lepton Yukawa couplings, can always be chosen flavour diagonal.

Having specified the basis, the $U(2)^5$ limit is described by a total of 124 (123 if not considering C_ϕ) independent Wilson coefficients [8]. As in the $U(3)^5$ case, the relations

X^3	ϕ^6 and $\phi^4 D^2$	$\psi^2 \phi^3$
$\mathcal{O}_G = f^{ABC} G_\mu^{A\nu} G_\nu^{B\rho} G_\rho^{C\mu}$ $\mathcal{O}_W = \varepsilon^{IJK} W_\mu^{I\nu} W_\nu^{J\rho} W_\rho^{K\mu}$	$\mathcal{O}_\phi = (\phi^\dagger \phi)^3$ $\mathcal{O}_{\phi\Box} = (\phi^\dagger \phi) \Box (\phi^\dagger \phi)$ $\mathcal{O}_{\phi D} = (\phi^\dagger D^\mu \phi)^* (\phi^\dagger D_\mu \phi)$	$\mathcal{O}_{e\phi}^{[pr]} = (\phi^\dagger \phi) (\bar{l}_p \phi e_r)$ $\mathcal{O}_{u\phi}^{[pr]} = (\phi^\dagger \phi) (\bar{q}_p \tilde{\phi} u_r)$ $\mathcal{O}_{d\phi}^{[pr]} = (\phi^\dagger \phi) (\bar{q}_p \phi d_r)$
$X^2 \phi^2$	$\psi^2 X \phi$	$\psi^2 \phi^2 D$
$\mathcal{O}_{\phi G} = \phi^\dagger \phi G_{\mu\nu}^A G^{A\mu\nu}$ $\mathcal{O}_{\phi W} = \phi^\dagger \phi W_{\mu\nu}^I W^{I\mu\nu}$ $\mathcal{O}_{\phi B} = \phi^\dagger \phi B_{\mu\nu} B^{\mu\nu}$ $\mathcal{O}_{\phi WB} = \phi^\dagger \tau^I \phi W_{\mu\nu}^I B^{\mu\nu}$	$\mathcal{O}_{eW}^{[pr]} = (\bar{l}_p \sigma^{\mu\nu} e_r) \tau^I \phi W_{\mu\nu}^I$ $\mathcal{O}_{eB}^{[pr]} = (\bar{l}_p \sigma^{\mu\nu} e_r) \phi B_{\mu\nu}$ $\mathcal{O}_{uG}^{[pr]} = (\bar{q}_p \sigma^{\mu\nu} T^A u_r) \tilde{\phi} G_{\mu\nu}^A$ $\mathcal{O}_{uW}^{[pr]} = (\bar{q}_p \sigma^{\mu\nu} u_r) \tau^I \tilde{\phi} W_{\mu\nu}^I$ $\mathcal{O}_{uB}^{[pr]} = (\bar{q}_p \sigma^{\mu\nu} u_r) \tilde{\phi} B_{\mu\nu}$ $\mathcal{O}_{dG}^{[pr]} = (\bar{q}_p \sigma^{\mu\nu} T^A d_r) \phi G_{\mu\nu}^A$ $\mathcal{O}_{dW}^{[pr]} = (\bar{q}_p \sigma^{\mu\nu} d_r) \tau^I \phi W_{\mu\nu}^I$ $\mathcal{O}_{dB}^{[pr]} = (\bar{q}_p \sigma^{\mu\nu} d_r) \phi B_{\mu\nu}$	$\mathcal{O}_{\phi l}^{(1)[pr]} = (\phi^\dagger i \overleftrightarrow{D}_\mu \phi) (\bar{l}_p \gamma^\mu l_r)$ $\mathcal{O}_{\phi l}^{(3)[pr]} = (\phi^\dagger i \overleftrightarrow{D}_\mu^I \phi) (\bar{l}_p \tau^I \gamma^\mu l_r)$ $\mathcal{O}_{\phi e}^{[pr]} = (\phi^\dagger i \overleftrightarrow{D}_\mu \phi) (\bar{e}_p \gamma^\mu e_r)$ $\mathcal{O}_{\phi q}^{(1)[pr]} = (\phi^\dagger i \overleftrightarrow{D}_\mu \phi) (\bar{q}_p \tau^I \gamma^\mu q_r)$ $\mathcal{O}_{\phi q}^{(3)[pr]} = (\phi^\dagger i \overleftrightarrow{D}_\mu^I \phi) (\bar{q}_p \tau^I \gamma^\mu q_r)$ $\mathcal{O}_{\phi u}^{[pr]} = (\phi^\dagger i \overleftrightarrow{D}_\mu \phi) (\bar{u}_p \gamma^\mu u_r)$ $\mathcal{O}_{\phi d}^{[pr]} = (\phi^\dagger i \overleftrightarrow{D}_\mu \phi) (\bar{d}_p \gamma^\mu d_r)$ $\mathcal{O}_{\phi ud}^{[pr]} = (\tilde{\phi}^\dagger i D_\mu \phi) (\bar{u}_p \gamma^\mu d_r)$
$(\bar{L}L)(\bar{L}L)$	$(\bar{R}R)(\bar{R}R)$	$(\bar{L}L)(\bar{R}R)$
$\mathcal{O}_{ll}^{[prst]} = (\bar{l}_p \gamma_\mu l_r) (\bar{l}_s \gamma^\mu l_t)$ $\mathcal{O}_{qq}^{(1)[prst]} = (\bar{q}_p \gamma_\mu q_r) (\bar{q}_s \gamma^\mu q_t)$ $\mathcal{O}_{qq}^{(3)[prst]} = (\bar{q}_p \gamma_\mu \tau^I q_r) (\bar{q}_s \gamma^\mu \tau^I q_t)$ $\mathcal{O}_{lq}^{(1)[prst]} = (\bar{l}_p \gamma_\mu l_r) (\bar{q}_s \gamma^\mu q_t)$ $\mathcal{O}_{lq}^{(3)[prst]} = (\bar{l}_p \gamma_\mu \tau^I l_r) (\bar{q}_s \gamma^\mu \tau^I q_t)$	$\mathcal{O}_{ee}^{[prst]} = (\bar{e}_p \gamma_\mu e_r) (\bar{e}_s \gamma^\mu e_t)$ $\mathcal{O}_{uu}^{[prst]} = (\bar{u}_p \gamma_\mu u_r) (\bar{u}_s \gamma^\mu u_t)$ $\mathcal{O}_{dd}^{[prst]} = (\bar{d}_p \gamma_\mu d_r) (\bar{d}_s \gamma^\mu d_t)$ $\mathcal{O}_{eu}^{[prst]} = (\bar{e}_p \gamma_\mu e_r) (\bar{u}_s \gamma^\mu u_t)$ $\mathcal{O}_{ed}^{[prst]} = (\bar{e}_p \gamma_\mu e_r) (\bar{d}_s \gamma^\mu d_t)$ $\mathcal{O}_{ud}^{(1)[prst]} = (\bar{u}_p \gamma_\mu u_r) (\bar{d}_s \gamma^\mu d_t)$ $\mathcal{O}_{ud}^{(8)[prst]} = (\bar{u}_p \gamma_\mu T^A u_r) (\bar{d}_s \gamma^\mu T^A d_t)$	$\mathcal{O}_{le}^{[prst]} = (\bar{l}_p \gamma_\mu l_r) (\bar{e}_s \gamma^\mu e_t)$ $\mathcal{O}_{lu}^{[prst]} = (\bar{l}_p \gamma_\mu l_r) (\bar{u}_s \gamma^\mu u_t)$ $\mathcal{O}_{ld}^{[prst]} = (\bar{l}_p \gamma_\mu l_r) (\bar{d}_s \gamma^\mu d_t)$ $\mathcal{O}_{qe}^{[prst]} = (\bar{q}_p \gamma_\mu q_r) (\bar{e}_s \gamma^\mu e_t)$ $\mathcal{O}_{qu}^{(1)[prst]} = (\bar{q}_p \gamma_\mu q_r) (\bar{u}_s \gamma^\mu u_t)$ $\mathcal{O}_{qu}^{(8)[prst]} = (\bar{q}_p \gamma_\mu T^A q_r) (\bar{u}_s \gamma^\mu T^A u_t)$ $\mathcal{O}_{qd}^{(1)[prst]} = (\bar{q}_p \gamma_\mu q_r) (\bar{d}_s \gamma^\mu d_t)$ $\mathcal{O}_{qd}^{(8)[prst]} = (\bar{q}_p \gamma_\mu T^A q_r) (\bar{d}_s \gamma^\mu T^A d_t)$
$(\bar{L}R)(\bar{L}R)$	$(\bar{L}R)(\bar{R}L)$	
$\mathcal{O}_{quqd}^{(1)[prst]} = (\bar{q}_p^i u_r) \epsilon_{ij} (\bar{q}_s^j d_t)$ $\mathcal{O}_{quqd}^{(8)[prst]} = (\bar{q}_p^i T^A u_r) \epsilon_{ij} (\bar{q}_s^j T^A d_t)$ $\mathcal{O}_{lequ}^{(1)[prst]} = (\bar{l}_p^i e_r) \epsilon_{ij} (\bar{q}_s^j u_t)$ $\mathcal{O}_{lequ}^{(3)[prst]} = (\bar{l}_p^i \sigma_{\mu\nu} e_r) \epsilon_{ij} (\bar{q}_s^j \sigma^{\mu\nu} u_t)$	$\mathcal{O}_{ledq}^{[prst]} = (\bar{l}_p^i e_r) (\bar{d}_s q_{ti})$	

Table 1. Dimension-6 operators in the Warsaw basis, adapted from ref. [32]. We collectively denote by X the field strength tensors of the SM gauge group ($X = G^{\mu\nu}, W^{\mu\nu}, B^{\mu\nu}$), by ψ a generic fermion field, and by ϕ the scalar field of the SM. Among the fermion fields, q and l denote $SU(2)_L$ left-handed doublets while u, d, e $SU(2)_L$ right-handed singlets, with family indices specified by the superscript in square brackets.

between the $U(2)^5$ Wilson coefficients and those of the general SMEFT are presented in Appendix A.2, which also sets the notation for the presentation of the $U(2)^5$ -symmetric results, following ref. [15].

2.2 Renormalization group evolution in the SMEFT

Assuming that the SMEFT coefficients are generated by BSM physics at the UV scale Λ , the Wilson coefficients at the EW scale μ_W are obtained by running them from the UV scale Λ to the EW scale μ_W using the leading order (LO) RG equations derived in refs. [36–38]. Lacking the next-to-leading SMEFT anomalous dimension, we can control only log-enhanced higher-order corrections to SMEFT contributions. Hence, we use tree-level matching conditions and matrix elements, and compute all SMEFT Wilson coefficients at a common scale μ_W that for convenience we choose to be $\mu_W = M_W$. For all high- p_T observables (Higgs, top, and Drell-Yan), we use the same scale μ_W , since the difference between the relevant physical scale of those processes and M_W is such that no large logarithms arise, except for a few regions of phase space which currently still have large experimental uncertainties.

Working at linear order in the SMEFT coefficients, we can write the Wilson coefficients at the EW scale μ_W as:

$$C_i(\mu_W) = U(\mu_W, \Lambda)_{ij} C_j(\Lambda), \quad (2.2)$$

where $U(\mu_W, \Lambda)$ is the evolver between the scales Λ and μ_W computed neglecting the effect of SMEFT coefficients in the running of the SM parameters. At this order, one would still need to recompute the evolver $U(\mu_W, \Lambda)$ for each given value of the SM parameters in the Monte Carlo integration. However, as stated above, at linear order we can neglect the effect of the SMEFT in the extraction of the SM parameters from experimental measurements when computing $U(\mu_W, \Lambda)$. This further justifies neglecting also the small uncertainties on SM parameters in the computation of $U(\mu_W, \Lambda)$, so that the evolver becomes a constant matrix for fixed μ_W and Λ , allowing for a dramatic increase in the speed of the numerical computation of the Wilson coefficients at the scale μ_W .

Concerning the SM parameters, in principle one could just define them at the scale Λ , evolve them to the EW scale μ_W using the full SMEFT, and then use the measurements of masses and couplings as constraints. However, this is extremely inefficient for the parameters that are very precisely determined experimentally, such as G_F , M_Z , α and the lepton masses. For this reason, we follow the same approach as in SM EW precision physics and choose to express all observables in terms of a set of input parameters, namely G_F , α or M_W , M_Z , M_h and the lepton masses. This amounts to trading implicitly the values of the SM parameters at the EW scale, including the corrections from the SMEFT, for the chosen set of input values. Of course, care must be taken in the EW sector, where the SM relations between masses and couplings are modified by the SMEFT.

One could be tempted to apply the same procedure to quark masses and CKM angles [39]. However, one of the symmetry assumptions we are using, namely exact $U(2)^5$ for $d = 6$ SMEFT operators, requires specifying the structure of the SM Yukawa couplings at the scale Λ , and the relations between quark masses, CKM angles, and Yukawa couplings are modified by SMEFT contributions. Thus, one cannot just trade the experimental values of quark masses and CKM angles for the corresponding SM parameters at the EW

scale, and keeping the SMEFT contributions in the Yukawa matrices RGE is essential.¹ To impose the required flavour structure, we choose as parameters in the quark flavour sector the Yukawa couplings at the scale Λ , which are then evolved to the EW scale including the effect of the SMEFT in the running. Once evolved to the EW scale, the Yukawa couplings are used to compute the quark masses and CKM angles, including SMEFT contributions, which are then compared to the experimental values. Concerning the leptons, since we are assuming diagonal Yukawa couplings for the charged leptons and individual lepton numbers are preserved, the flavour orientation at the scale Λ is irrelevant and, as stated above, we can trade the lepton Yukawa couplings at the EW scale for the corresponding masses.

The RG evolution from the scale Λ to μ_W is performed within the `HEPfit` framework using the `RGEsolver` library [40]. The SMEFT Lagrangian at the scale μ_W is then expanded around the minimum of the scalar potential, and the quark mass matrices are diagonalised through the biunitary transformations

$$M_{u,d} = V_{u,d}^R M_{u,d}^{\text{diag}} V_{u,d}^{L\dagger}. \quad (2.3)$$

The SMEFT operators involving quark fields are then transformed to the mass eigenstate basis using the matrices $V_{u,d}^{L,R}$ after removing unphysical phases. The unitary CKM matrix is defined as $V_{\text{CKM}} \equiv V_u^{L\dagger} V_d^L$.² The SMEFT coefficients in the mass eigenstate basis are then used to compute the observables at the scale μ_W .³ Most observables in the flavour sector involve lower energies, and are therefore computed in the LEFT, where the massive gauge bosons, the Higgs field and the top quark are integrated out. The matching between the two EFT's, the SMEFT and the LEFT, is implemented according to ref. [29]. For each flavour observable, as detailed in Section 3.6, the LEFT coefficients are evolved to the relevant energy scale using the LEFT RG equations.

3 Constraints on new physics from current data

We perform a global fit of the SMEFT including EW, Drell-Yan, Higgs-boson, top-quark, and flavour observables. The fit has been implemented in the `NPSMEFTd6General` model of the open-source `HEPfit` framework [30, 31]. In this section, after specifying the adopted statistical framework and fitting procedure, we describe the methods used for the calculation of the different classes of observables entering the fit and provide references for the corresponding experimental measurements.

3.1 Introduction to the fitting procedure

We perform a Bayesian analysis to extract the posterior probability density for the SMEFT coefficients $C_i(\Lambda)$ given the experimental data, a uniform prior for $C_i(\Lambda)$ in the $[-4\pi, 4\pi] \sim$

¹To our knowledge, these corrections have been neglected in all the SMEFT fits that have considered the RGE evolution of the SMEFT coefficients so far.

²Note that the determination of the CKM matrix elements from the experimental data is affected by additional corrections from SMEFT operators contributing to the relevant CKM observables. All these potential new physics effects are included in our calculations.

³Under our flavour assumptions, the flavour rotation is expected to have a negligible effect for the calculation of flavour-diagonal observables such as EW, Higgs boson, and top quark observables.

$[-15, 15]$ perturbative range⁴, and a Gaussian prior for the input parameters G_F , α or M_W (depending on the input scheme), M_Z , M_h , $\alpha_s(M_Z)$ and the lepton masses, as described in Section 2.2. Concerning instead quark masses and CKM matrix elements, we consider uniform priors in the ranges reported in Table 2, and use the experimental information to constrain the relevant combination of SM parameters and SMEFT coefficients. SM parameters are always floating in the fit, while for SMEFT coefficients we perform fits with one operator at a time and fits with all coefficients floating simultaneously. To assess the impact of the different sets of observables, we also perform fits excluding one set at a time, and determine in this way which observables gives the strongest constraint. For each fit, the probability density function (pdf) of the SMEFT coefficients $C_i(\Lambda)$ is sampled using its numerical representation through the Markov Chain Monte Carlo (MCMC) implemented in `HEPfit` using the `BAT` library [43]. From the MCMC samples, we compute 68% and 95% Highest Posterior Density Intervals (HPDI) for the SMEFT coefficients. From the largest absolute value of the 95% HPDI we compute the lower bound on the effective NP interaction scale $\Lambda/\sqrt{|C|}$.

Parameter	Range	Parameter	Range
$m_t(m_t)$	[155, 171] GeV	λ_{CKM}	[0.223, 0.227]
$m_b(m_b)$	[3.776, 4.616] GeV	A_{CKM}	[0.81, 0.83]
$m_c(m_c)$	[1.24, 1.34] GeV	$\bar{\rho}_{\text{CKM}}$	[0.165, 0.185]
$m_s(2 \text{ GeV})$	[88, 98] MeV	$\bar{\eta}_{\text{CKM}}$	[0.365, 0.385]
$m_d(2 \text{ GeV})$	[4.4, 5.0] MeV		
$m_u(2 \text{ GeV})$	[1.9, 2.5] MeV		

Table 2. Ranges of the SM-parameter uniform priors used in the fits. The values of the quark masses are given at the corresponding renormalization scale, as indicated in the table. The CKM parameters are defined in the Wolfenstein parametrisation [44].

3.2 General setup for theoretical predictions

All the observables considered in the global fit are consistently calculated up to linear terms in the SMEFT Wilson coefficients⁵. Establishing the validity of the SMEFT expansion at linear order is certainly important, and estimating it by including quadratic effects (i.e. terms of $O(1/\Lambda^4)$ originating from dimension-6 operators), although not sufficient to prove such validity, can provide partial information. Nevertheless, given the scope of our study, which presents for the first time a global fit of the SMEFT including EW, Drell-Yan, Higgs-boson, top-quark, and flavour observables, with SMEFT Wilson coefficients and SM parameters simultaneously floating and full RGE effects taken into account, we deem it appropriate to focus on a consistent implementation of the SMEFT at linear order and address the effect of quadratic terms in future studies.

⁴This limit can be understood by demanding that a loop contribution from dimension-6 operators gives a contribution not larger than a genuine dimension-eight operator, and so forth for higher and higher dimensions. This is satisfied for $C_i \lesssim 4\pi$, following naive dimensional analysis [41, 42].

⁵In the `HEPfit` framework this corresponds to using the `NPSMEFTd6General` model setting the `QuadraticTerms` flag to false.

Given a choice of input parameters $\{p\}$, all observables are expressed in terms of the input-parameter experimental values $\{\tilde{p}\}$ ($\tilde{p} = p + \delta p_{\text{SMEFT}}$),

$$\mathcal{O}(\{\tilde{p}\}) = [\mathcal{O}_{\text{SM}}(\{p\}) + \delta\mathcal{O}_{\text{SMEFT}}(\{p\})]_{\{p\} \rightarrow \{\tilde{p}\}}, \quad (3.1)$$

where SMEFT linear contributions come from the linear-order terms in both the $\delta\mathcal{O}_{\text{SMEFT}}(\{p\})$ direct contribution and from expressing $p = p(\{\tilde{p}\})$ in terms of measured input parameters in $\mathcal{O}_{\text{SM}}(\{p\})$. Choosing a given input scheme modifies the dependence of $\mathcal{O}(\{\tilde{p}\})$ on SMEFT coefficients. We note that for the purpose of illustration all the results presented in Section 4 have been obtained in the M_W -scheme, which is commonly used for global fits that include a majority of collider observables.⁶

Using Eq. (3.1), for all the observables considered in our study we have implemented state-of-the-art SM predictions (including QCD and EW corrections that could be analytically or numerically parametrised in an efficient way in the code) while SMEFT corrections, obtained from the interference between SMEFT and SM amplitudes, have been calculated at the lowest perturbative order. For several observables, e.g. the high- p_T processes in top-quark physics, these are rescaled by the effect of higher-order SM corrections, assuming that their effects in the SM and the SMEFT are similar. When needed, further details will be given in the following sections where we discuss specific sets of observables.

3.3 Electroweak and Drell-Yan observables

We include in the fits the whole set of EW precision observables measured at the Z pole at LEP/SLC.⁷ A thorough description of all elements entering the EW global fit, including references to the state-of-the-art theoretical parametrisations used in `HEPfit`, is given in refs. [46, 47], to which we refer the reader interested in such details.

For the W mass we consider the inputs from LEP2, ATLAS, CMS, LHCb and Tevatron, excluding the recent CDF measurement [48] which, in the light of the very recent CMS result [49], requires additional investigation.⁸ We combine all the hadronic W -mass measurements obtained using the CT18 PDF set, assuming the same PDF correlation indicated in [50], which we take to be the same for ATLAS and CMS (not present in that reference). We also assume that QED systematics are 100% correlated across the different measurements. The hadron-collider result is then combined with the LEP2 W -mass determination in an uncorrelated manner. This results in an average value $M_W = 80.3635 \pm 0.0080$ GeV. Similarly, we combine the measurements of the W width results from LEP2, ATLAS

⁶The only exceptions are the predictions for LHC Drell-Yan observables which, as will be explained below, are computed with the `HighPT` package [45]. These are given in the α -scheme. Given that the difference between the α and M_W schemes involves only operators that are well constrained by EW and Higgs precision observables, while the high-energy Drell-Yan measurements target four-fermion interactions, we expect this scheme mismatch to have a very small effect in the results.

⁷We use the results obtained without assuming lepton universality.

⁸In ref. [47] we discussed the impact of the CDF measurement on the EW precision fit, and introduced a *conservative* scenario in which the uncertainty on the M_W average including CDF was inflated to ensure compatibility among experimental measurements. This is less justified after the very recent CMS result, whose accuracy is comparable to the CDF one but is fully consistent with all existing measurements except for the CDF one.

and Tevatron. There is some tension between the ATLAS and Tevatron determinations ($\chi^2/\text{d.o.f.} \approx 3$), which we take into account by scaling the uncertainty of the combination, before adding the LEP2 result. Finally, since the measurements of the W width are not available for all experiments providing results for M_W , we neglect the correlation between the two observables. We obtain $\Gamma_W = 2.151 \pm 0.049$ GeV. For the Z -boson mass, we also take into account the CDF determinations in ref. [48], in good agreement with the LEP value. The Higgs-boson mass completes the list of SM inputs needed in the W -mass scheme, and here we use the same value as in ref. [47]. The numerical values used in the fit for those observables directly related to the SM inputs are reported in Table 3.⁹

Observable	Experimental value	Observable	Experimental value
M_W (GeV)	80.3635 ± 0.0080	M_Z (GeV)	91.1880 ± 0.0020
M_h (GeV)	125.1 ± 0.09	$\alpha_s(M_Z)$	0.11873 ± 0.00056
m_t^{pole} (GeV)	172.61 ± 0.59	$m_b(m_b)$ (GeV)	4.196 ± 0.014
$m_c(m_c)$ (GeV)	1.2917 ± 0.0048	$m_s(2 \text{ GeV})$ (MeV)	93.14 ± 0.55
$m_d(2 \text{ GeV})$ (MeV)	4.70 ± 0.04	$m_u(2 \text{ GeV})$ (MeV)	2.20 ± 0.06

Table 3. Observables relevant for the determination of the SM input parameters used in the fits (in the W mass scheme). The values of the quark masses are taken from FLAG averages [51]. For $\alpha_s(M_Z)$ we use the recent lattice QCD result of ref. [52]. See the text for details on the W mass and width.

Measurements of the W branching ratios are also included, both from LEP2 [53] and from the recent (and more precise) determination by CMS [54]. We also include the measurements available for ratios of W and Z decays into different lepton flavours from Tevatron [55–58] and LHC [59–62], which serve as tests of lepton flavour universality.

Two-to-two fermion processes above the Z pole are also considered in our analysis. First, we include the measurements of total cross section and asymmetries for the $e^+e^- \rightarrow \mu^+\mu^-, \tau^+\tau^-$ channels, the hadronic cross section, and the differential cross sections in $e^+e^- \rightarrow e^+e^-$ taken from LEP2 [53].¹⁰ Di-lepton ($\ell^+\ell^-$) and single-lepton ($\ell\nu$) processes from LHC Drell-Yan measurements are also included, implementing in `HEPfit` the predictions from `HighPT` [45]. These two-to-two fermion processes measured at high energies are largely sensitive to four-fermion operators, since their effects grow with the energy.

Finally, we also include in our study the constraints from W^+W^- production at LEP2. For this observable we take into account the information available for the inclusive and differential cross sections measured at energies between 189 and 208 GeV, following the study in [63].

⁹The Fermi constant G_F , known to a significantly higher precision, is fixed in the fits.

¹⁰On the hadronic side, we do not include the measurements of R_b and R_c , since each is derived assuming the other is SM-like, which in general will not be true in the SMEFT.

3.4 Higgs-boson observables

We consider the full combination of Higgs-boson signal strengths at 8 TeV from ATLAS and CMS as presented in ref. [64] as well as the most recent combined measurements of Higgs-boson production cross sections, decay branching ratios, and simplified template cross sections (STXS) as provided by the ATLAS and CMS collaborations using 139 fb^{-1} of collision data at $\sqrt{s} = 13 \text{ TeV}$ [25, 33, 65–68]. All measurements are separated by production and decay modes. These include measurements of Higgs-boson production via gluon-gluon fusion (ggF), vector-boson fusion (VBF), and associated production with gauge bosons (ZH and WH) and top quarks ($t\bar{t}H$ and tH) as well as measurements of Higgs-boson decays into $\gamma\gamma$, ZZ^* , WW^* , $\tau^+\tau^-$, $b\bar{b}$, $\mu^+\mu^-$, and $Z\gamma$. For the STXS we adopt the most recent Stage 1.2 binning and compare with the experimental results presented in [25, 68]. In all cases we include the full correlation matrices provided by the experimental collaborations.

We parametrise both cross sections and decay rates at linear order in the SMEFT coefficients using `MG5_aMC@NLO` [69] with a UFO file developed for this study.¹¹ To obtain the parametrisation of some SM loop-induced processes, e.g. ggF, we also use the `SMEFT@NLO` package [73].

As mentioned earlier, we work in the M_W -scheme and use as default input parameters the experimental values of G_F , M_Z , and M_W . We adopt the NNPDF4.0 NLO set of parton distribution functions with $\alpha_s(M_Z) = 0.118$ and fix factorisation and renormalization scales to the relevant scale for each process (e.g. $\mu = M_H$ for ggF, etc.). All chosen scales are very close to μ_W , the scale at which we evaluate the RG-evolved SMEFT Wilson coefficients such that, for the purpose of this study, the effects of running from μ_W to the actual scale at which the Higgs-boson production processes have been calculated is negligible, specially given the experimental uncertainty on the high- p_T bins.¹² Likewise, the theoretical error induced by the choice of PDF and their variation (at the few per-cent level for most state-of-the-art SM calculations) is also below the sensitivity of our study.

The parametrisation of the STXS has been obtained at parton level. For the purpose of the SMEFT global fit, working at parton level captures the bulk of the relevant SMEFT effects. Indeed, we did not notice any substantial difference from the parametrisations reported e.g. in [65] where parton-shower effects have been fully simulated, except for a few bins that could not be obtained at parton level. This includes for instance the case of ggF Higgs-boson production with 0 jets (where the STXS bin is defined by a cut on the Higgs-boson transverse momentum) or the case of Higgs-boson plus two jets final states (where the STXS bins are defined by a cut on the transverse momenta of the whole final-state system) since in both cases the transverse momentum used to define the STXS bin cannot be properly defined without considering extra final-state partons as produced by the parton-shower. In these cases we have removed the corresponding bin.

¹¹The UFO file used for this study has been generated with the `SMEFTci2` Mathematica in-house code. This is based on `SMEFTsim` [70, 71] and has also been validated against `SmeftFR v3` [72].

¹²As shown in Ref. [74] (also recently revisited in Ref. [75]) these effects are not critical given the current experimental precision but may be relevant in the near future when data from HL-LHC becomes available.

3.5 Top-quark observables

Process	Observable	\sqrt{s}	$\int \mathcal{L}$	SM	Ref.
$p\bar{p} \rightarrow t\bar{t}$	$dA_{\text{FB}}^{t\bar{t}}/dm_{t\bar{t}}$	1.96 TeV	9.7 fb ⁻¹	[76, 77]	[78]
$pp \rightarrow t\bar{t}$	$\sigma_{t\bar{t}}^{13\text{TeV}}/\sigma_{t\bar{t}}^{8\text{TeV}}$	13 & 8 TeV	20 & 36 fb ⁻¹		[81]
	$\sigma_{t\bar{t}}^{8\text{TeV}}/\sigma_{t\bar{t}}^{7\text{TeV}}$	8 & 7 TeV	20 & 5 fb ⁻¹		[82]
	$\sigma_{t\bar{t}}$	13 TeV	36/139 fb ⁻¹	[79, 80]	[81, 83]
	$d\sigma_{t\bar{t}}/dm_{t\bar{t}}$	13 TeV	36 fb ⁻¹		[84]
	$(d\sigma_{t\bar{t}}/dm_{t\bar{t}})/\sigma_{t\bar{t}}$	13 TeV	36/137 fb ⁻¹		[85, 86]
	$dA_C/dm_{t\bar{t}}$	13 TeV	140 fb ⁻¹		[87]
$pp \rightarrow t\bar{t}Z$	$d\sigma/dp_T^Z$	13 TeV	77.5/140 fb ⁻¹	[88]	[89]/[90]
$pp \rightarrow t\bar{t}\gamma$	$d\sigma/dp_T^\gamma$	13 TeV	140 fb ⁻¹	[91, 92]	[93–95]
$pp \rightarrow t\bar{t}W$	σ_{ttW^\pm} $\sigma_{ttW^+}/\sigma_{ttW^-}$	13 TeV	140 fb ⁻¹	[96, 97]	[98, 99]
$t \rightarrow Wb$	F_0, F_L	8 TeV	20 fb ⁻¹		[101]
		13 TeV	140 fb ⁻¹	[100]	[102]
$pp \rightarrow tW$	σ	7 TeV	4.6 & 1.5 fb ⁻¹	[103]	[104]
		8 TeV	20 fb ⁻¹	[103]	[104]
		13 TeV	3.2/140 fb ⁻¹	[103]	[105]/[106]
$pp \rightarrow t\bar{b}$ (s-ch)	σ	8 TeV	20 fb ⁻¹		[104]
		13 TeV	140 fb ⁻¹	[107, 108]	[109, 110]
$pp \rightarrow tq$ (t-ch)	σ	7 TeV	4.6 & 1.5 fb ⁻¹		[104]
		8 TeV	20 fb ⁻¹	[107, 108]	[104]
		13 TeV	36/140 fb ⁻¹		[111]/[112]
$pp \rightarrow t\gamma q$	σ	13 TeV	140/36 fb ⁻¹	[69]	[113]/[114]
$pp \rightarrow tZq$	σ	13 TeV	140 fb ⁻¹	[69]	[115, 116]
$pp \rightarrow t\bar{t}b\bar{b}$	σ	13 TeV	36 fb ⁻¹	[69]	[117]
$pp \rightarrow t\bar{t}t\bar{t}$	σ	13 TeV	140 fb ⁻¹	[118]	[119–121]

Table 4. Measurements of top-quark observables included in the SMEFT fit. For each measurement we give: the process, the observable, the center-of-mass energy, and the integrated luminosity. The last two columns list the references for the SM predictions and measurements that are included in the fit.

The top-quark interactions have been characterised with excellent precision by the Tevatron and the LHC. Our top-quark data set, summarised in Table 4, contains the most relevant and updated top-quark measurements. This data set consists of differential measurements of top-quark pair production, including also the $t\bar{t}$ charge asymmetry at LHC and the forward-backward asymmetry at Tevatron, differential and inclusive measurements of top-quark production in association with EW boson,¹³ EW single top-quark production

¹³The associated production with Higgs bosons is listed in Section 3.4 and, therefore, not listed here.

measurements, helicity measurements of top-quark decays, and four heavy quark production measurements including four top-quark production and two top-quark production in association with two bottom quarks.¹⁴

In the top-quark sector, the theoretical uncertainties can be sizable and comparable to the experimental ones, particularly for differential measurements. To ensure a reliable analysis, we have taken both theoretical and experimental uncertainties into account. Furthermore, for the differential measurements, we have also included the correlations among the different bins, providing a complete and accurate treatment of the uncertainties.

As in the case of Higgs-boson observables, top-quark observables are also parametrised at linear order in the SMEFT coefficients using `MG5_aMC@NLO` with the same UFO file, PDF, and scale choices as described in Section 3.4. In this case, however, we have included differential distributions for the $pp \rightarrow t\bar{t}$ process with invariant masses reaching up to a few TeV. As shown in ref. [125], the most suitable dynamical scale for such differential observables is $H_T/4 = \frac{1}{4} \left(\sqrt{m_t^2 + p_{T,t}^2} + \sqrt{m_t^2 + p_{T,\bar{t}}^2} \right)$, which is below one quarter of the invariant mass of the $t\bar{t}$ system. Hence, even for the highest invariant mass bins, the optimal scale choice remains at a few hundred GeV, comparable to the fixed scale μ_W used for the other observables. This suggests that the deviation introduced by using μ_W instead of the optimal dynamic scale should lie within the theoretical uncertainty of our predictions, thereby justifying the choice of keeping μ_W also for this sector.

3.6 Flavour observables

We now discuss in detail the procedure followed to study the constraints arising in the flavour sector. The floating SM parameters are the CKM matrix elements and the quark masses. The fit involves also a set of hadronic parameters reported in Table 5 that can be computed in lattice QCD without (or with negligible) effects from the SMEFT.¹⁵

In the computation of all flavour observables, the SM contribution is evaluated using all available higher-order corrections to achieve the best possible accuracy. The SMEFT Lagrangian is matched to the LEFT at the scale μ_W using the results of ref. [29]. The LEFT coefficients are then evolved to the relevant energy scale using the LEFT renormalization group equations [126].

3.6.1 $\Delta F = 2$ observables

The most general $\Delta F = 2$ effective Hamiltonian involves $5 + 3$ operators [138]. However, in the context of the SMEFT, only $3 + 1$ of them are generated, namely, in the notation of ref. [138]:

$$Q_1^{q_i q_j} = (\bar{q}_i^\alpha \gamma_\mu P_L q_j^\alpha) (\bar{q}_i^\beta \gamma^\mu P_L q_j^\beta),$$

¹⁴A subset of these observables have been previously implemented in `HEPfit` to study specifically the top-quark sector [122–124].

¹⁵Results obtained fixing the lattice spacing using hadron spectroscopy are not affected by SMEFT contributions. In addition, there is usually good agreement (within current uncertainties) among results obtained fixing the lattice spacing with spectroscopy or with the weak decay constants, the latter procedure being potentially affected by SMEFT contributions. We conclude that within current uncertainties we can safely use all available lattice results.

$$\begin{aligned}
Q_4^{q_i q_j} &= (\bar{q}_i^\alpha P_L q_j^\alpha)(\bar{q}_i^\beta P_R q_j^\beta), \\
Q_5^{q_i q_j} &= (\bar{q}_i^\alpha P_L q_j^\beta)(\bar{q}_i^\beta P_L q_j^\alpha), \\
\tilde{Q}_1^{q_i q_j} &= (\bar{q}_i^\alpha \gamma_\mu P_R q_j^\alpha)(\bar{q}_i^\beta \gamma^\mu P_R q_j^\beta),
\end{aligned} \tag{3.2}$$

where $q_i = u_i, d_i$ are up- and down-type quark fields, $P_{L,R} = (1 \mp \gamma_5)/2$ are the left- and right-handed projectors, and α, β are colour indices. Furthermore, within the $U(2)^5$ flavour assumption, the operator $\tilde{Q}_1^{q_i q_j}$ is negligible. In terms of the LEFT operators of ref. [29], the Wilson coefficients of the above operators are given by

$$\begin{aligned}
C_1^{q_i q_j} &= -C_{qq}^{V,LL[ijij]}, \\
C_4^{q_i q_j} &= C_{qq}^{V8,LR[ijij]}, \\
C_5^{q_i q_j} &= 2C_{qq}^{V1,LR[ijij]} - C_{qq}^{V8,LR[ijij]}/3, \\
\tilde{C}_1^{q_i q_j} &= -C_{qq}^{V,RR[ijij]}.
\end{aligned} \tag{3.3}$$

Parameter	Value	Ref.
F_{B_s} (GeV)	0.2301 ± 0.0012	[51]
F_{B_s}/F_{B_d}	1.208 ± 0.005	[51]
$B_{B_s}(4.2 \text{ GeV})$	0.888 ± 0.040	[51]
B_{B_s}/B_{B_d}	1.015 ± 0.021	[51]
$B_{B_s,4}(4.2 \text{ GeV})$	0.98 ± 0.08	[51]
$B_{B_s,5}(4.2 \text{ GeV})$	1.66 ± 0.13	[51]
$B_{B_d,4}(4.2 \text{ GeV})$	0.99 ± 0.08	[51]
$B_{B_d,5}(4.2 \text{ GeV})$	1.58 ± 0.18	[51]
$B_K(2 \text{ GeV})$	0.552 ± 0.012	[51]
$B_{K,4}(2 \text{ GeV})$	0.904 ± 0.053	[51]
$B_{K,5}(2 \text{ GeV})$	0.618 ± 0.114	[51]
$\phi_{\varepsilon_K} (^\circ)$	43.51 ± 0.05	[127]
$\bar{\kappa}_{\varepsilon_K}$	0.97 ± 0.02	[128]
$(\Delta M_K)^{\text{SM}} (\text{ns}^{-1})$	8.8 ± 3.6	[129]
$B_{D,1}(3 \text{ GeV})$	0.765 ± 0.025	[51]
$B_{D,4}(3 \text{ GeV})$	0.98 ± 0.06	[51]
$B_{D,5}(3 \text{ GeV})$	1.05 ± 0.09	[51]
F_D (GeV)	0.2120 ± 0.0007	[51]
$(\Delta M_D)^{\text{SM}} (\text{ps}^{-1})$	0.005 ± 0.005	[130]
f_K (GeV)	0.15611 ± 0.00021	[131]
f_K/f_π	1.1966 ± 0.0018	[131]
$\delta R_\pi^{\text{phys}}$	0.0153 ± 0.0019	[131]
$\delta P_{c,u}$	0.04 ± 0.02	[132]

Table 5. Key hadronic parameters floated in the theoretical prediction of flavour observables in our analysis. In particular, we report the values of bag parameters and meson decay constants, along with the long-distance contributions assumed for both K - and D -meson mixing and for $K \rightarrow \pi\nu\bar{\nu}$.

Observable	Value	Ref.
Δm_{B_s} (ps ⁻¹)	17.765 ± 0.006	[127, 133]
ϕ_s	-0.049 ± 0.019	[127, 133]
A_{sl}^s	-0.0006 ± 0.00028	[127, 133]
Δm_{B_d} (ps ⁻¹)	0.5069 ± 0.0019	[127, 133]
$S_{J/\psi K_S}$	0.692 ± 0.016	[127, 133, 134]
A_{sl}^d	-0.0021 ± 0.0017	[127, 133]
ΔM_K (ns ⁻¹)	5.293 ± 0.009	[127]
ϵ_K	$(2.228 \pm 0.011) \times 10^{-3}$	[127]
ϕ_{12}^M (°)	1.9 ± 1.6	[130]
$\text{BR}(B \rightarrow \tau\nu) \times 10^4$	1.09 ± 0.24	[127]
$\text{BR}(D \rightarrow \tau\nu) \times 10^4$	9.9 ± 1.2	[127]
$\text{BR}(D \rightarrow \mu\nu) \times 10^4$	3.981 ± 0.089	[127]
$\text{BR}(D_s \rightarrow \tau\nu) \times 10^3$	5.31 ± 0.11	[127]
$\text{BR}(D_s \rightarrow \mu\nu) \times 10^2$	5.37 ± 0.10	[127]
$\Gamma(K \rightarrow \mu\nu)/\Gamma(\pi \rightarrow \mu\nu)$	1.3367 ± 0.0029	[127]
$\text{BR}(\pi \rightarrow \mu\nu) \times 10^5$	3.8408 ± 0.0007	[127]
$d\Gamma(B \rightarrow D\ell\nu)/dw$	$[\Delta\Gamma_i/\Delta w]_{10 \times 10}$	[135]
$\text{BR}(K^+ \rightarrow \pi^+\nu\bar{\nu}) \times 10^{10}$	1.175 ± 0.365	[127]
$\text{BR}(B \rightarrow X_s\gamma) \times 10^4$	3.49 ± 0.19	[127]
$\overline{\text{BR}}(B_s \rightarrow \mu^+\mu^-) \times 10^9$	3.41 ± 0.29	[127]

Table 6. Experimental measurements used for all the flavour observables considered in the present analysis, along with the corresponding references. The set includes both $\Delta F = 1$ and $\Delta F = 2$ observables, which play a crucial role in constraining the parameters of the Unitarity Triangle analysis [136], testing the SM consistency, and probing potential contributions from NP [137].

For the relevant matrix elements we use the lattice B-parameters reported in Table 5. For $B_q - \bar{B}_q$ mixing ($q = d, s$), we use in the fit the mass difference, the time-dependent CP asymmetries, and the semileptonic asymmetries. For $K - \bar{K}$ mixing, we use the ϵ_K CP-violating parameter and the mass difference ΔM_K . For the SM contribution to the latter, we use the lattice QCD estimate in ref. [129]. Finally, for the dispersive phase of $D - \bar{D}$ mixing ϕ_{12}^M , we use the results of the global fit of ref. [130] and, lacking an estimate of the SM contribution to the real part of the amplitude, assume that the SM contribution can saturate the experimental value. All the experimental results used in this section are summarised in Table 6, while the expressions for the observables in terms of the operators in eq. (3.2) can be found for example in refs. [139, 140].

3.6.2 $\Delta F = 1$ observables

Several $\Delta F = 1$ processes enter our analysis for the purpose of determining the CKM matrix elements and constraining the SMEFT coefficients. Let us consider first the charged current leptonic decays, which include $\pi \rightarrow \mu\nu$, $K \rightarrow \mu\nu$, $B \rightarrow \tau\nu$, $D_{(s)} \rightarrow \tau\nu$, and $D_{(s)} \rightarrow \mu\nu$.

The relevant LEFT operators are given by

$$\begin{aligned}
Q_{vedu}^{VLL[kkij]} &= (\bar{\nu}_k \gamma_\mu P_L e_k) (\bar{d}_i \gamma^\mu P_L u_j), \\
Q_{vedu}^{VLR[kkij]} &= (\bar{\nu}_k \gamma_\mu P_L e_k) (\bar{d}_i \gamma^\mu P_R u_j), \\
Q_{vedu}^{SRR[kkij]} &= (\bar{\nu}_k P_R e_k) (\bar{d}_i P_R u_j), \\
Q_{vedu}^{SRL[kkij]} &= (\bar{\nu}_k P_R e_k) (\bar{d}_i P_L u_j), \\
Q_{vedu}^{TRR[kkij]} &= (\bar{\nu}_k \sigma_{\mu\nu} P_R e_k) (\bar{d}_i \sigma^{\mu\nu} P_R u_j).
\end{aligned} \tag{3.4}$$

After the RGE below the EW scale, the relevant matrix elements are computed using the lattice QCD results for the decay constants, including the QED corrections for light meson decays [131], as reported in Table 5. The experimental results used in this section are all summarised in Table 6.

For the process $B \rightarrow D\ell\nu$, the relevant matching conditions remain those corresponding to the operators shown in eq. (3.4). The corresponding matrix elements are computed using the Boyd-Grinstein-Lebed parameterization, employing a z -expansion truncated at second order in the conformal variable z . In this analysis, we incorporate constraints from lattice QCD given in [141] as well as unitarity bounds on the expansion coefficients. The experimental data used also include a 10×10 correlation matrix ($[\Delta\Gamma_i/\Delta w]_{10 \times 10}$), see reference in Table 6.

We now turn to the second class of $\Delta F = 1$ decays, namely the flavour-changing neutral current (FCNC) processes. In our analysis, we include two key decays that are particularly sensitive to potential contributions from BSM physics: the inclusive radiative decay $B \rightarrow X_s \gamma$ and the short-distance dominated exclusive decay $B_s \rightarrow \mu^+ \mu^-$. SM predictions for these processes are computed to next-to-next-to-leading order accuracy as detailed in references [142, 143]. The leading effects of NP for the inclusive radiative channel involve the following operators:

$$\begin{aligned}
Q_{d\gamma}^{[ij]} &= (\bar{d}_i \sigma_{\mu\nu} P_R d_j) F^{\mu\nu}, \\
Q_{dG}^{[ij]} &= (\bar{d}_i \sigma_{\mu\nu} T_A P_R d_j) G_A^{\mu\nu}, \\
Q_{ud}^{V1LL[ijkl]} &= (\bar{u}_i \gamma_\mu P_L u_j) (\bar{u}_k \gamma^\mu P_L d_l), \\
Q_{ud}^{V8LL[ijkl]} &= (\bar{u}_i \gamma_\mu T^A P_L u_j) (\bar{u}_k \gamma^\mu T^A P_L d_l), \\
Q_{ud}^{V1RR[ijkl]} &= (\bar{u}_i \gamma_\mu P_R u_j) (\bar{u}_k \gamma^\mu P_R d_l), \\
Q_{ud}^{V8RR[ijkl]} &= (\bar{u}_i \gamma_\mu T^A P_R u_j) (\bar{u}_k \gamma^\mu T^A P_R d_l),
\end{aligned}$$

where the current-current operators also contribute to the decay at leading order via one-loop running effects below the EW scale. On the other hand, the leading-order contributions of new physics in $B_s \rightarrow \mu^+ \mu^-$ are not affected by RGE effects below the EW scale and, in particular, are given by the tree-level matching of the SMEFT onto:

$$\begin{aligned}
Q_{ed}^{VLL[kkij]} &= (\bar{e}_k \gamma_\mu P_L e_k) (\bar{d}_i \gamma^\mu P_L d_j), \\
Q_{de}^{VLR[ijkk]} &= (\bar{d}_i \gamma_\mu P_L d_j) (\bar{e}_k \gamma^\mu P_R e_k).
\end{aligned}$$

Finally, we consider the FCNC process $K^+ \rightarrow \pi^+ \nu \bar{\nu}$, which is also theoretically clean and highly suppressed in the SM [144]. Due to its strong sensitivity to short-distance physics and minimal hadronic uncertainties [145], it provides a powerful probe of potential new physics effects. Assuming lepton universality and taking into account the flavour symmetries adopted in our study, the only LEFT operator relevant for this channel is:

$$Q_{\nu d}^{VLL[kkij]} = (\bar{\nu}_k \gamma_\mu P_L \nu_k) (\bar{d}_i \gamma^\mu P_L d_j).$$

4 Results

In this section, we present the results of the fits we performed with different assumptions on the SMEFT flavour symmetries, namely $U(3)^5$ and $U(2)^5$ in both the UP and DOWN bases defined in Section 2.1. In order to assess the impact of the RGE of the SMEFT Wilson coefficients, we give results for $\Lambda = 10$ and $\Lambda = 3$ TeV with RGE, and $\Lambda = 1$ TeV without RGE (labeled in the plots and tables as “noRGE”). Given the leading logarithmic accuracy of the RGE, to ensure the dominance of log-enhanced terms we require $\ln(\mu_1^2/\mu_2^2) \gtrsim 2$, and consequently we cannot resolve scale ratios smaller than ~ 3 , which justifies the chosen values of Λ . We perform both global fits with all SMEFT Wilson coefficients floating and fits varying one Wilson coefficient at a time (called *individual fits* in the following), while SM input parameters and hadronic matrix elements are always floated. For individual fits, we also perform fits omitting different sets of observables, to assess the impact of each set on the results. Numeric results for all the fits are reported in Appendix B, while here we illustrate them in a series of plots and discuss their main features and physical interpretation.

4.1 Results for the $U(3)^5$ flavour symmetric SMEFT

Assuming that NP respects the $U(3)^5$ flavour symmetry, the SMEFT coefficients at the scale Λ are given by eq. (A.1). Let us first consider individual fits. In Table 7 we report results for $\Lambda = 10$ TeV and $\Lambda = 3$ TeV including RGE, and for $\Lambda = 1$ TeV without RGE. For each coefficient we give the 68% HPDI interval and the bound on $\Lambda/\sqrt{|C_i|}$ obtained by taking the maximum of the 95% HPDI interval for $|C_i|$. The cases in which the posterior for the relevant Wilson coefficient is not centered around zero so that the 68% or 95% HPDI (from which the bound on $\Lambda/\sqrt{|C_i|}$ is obtained) touches the edges of the prior’s range (see Section 3.1) are indicated in red. The 68% HPDI intervals for the C_i roughly scale as Λ^2 up to RG effects, unless they hit the prior’s edges. Conversely, the bounds on the effective scale $\Lambda/\sqrt{|C_i|}$ only change due to RG effects and possibly due to the prior’s range. It happens for several less constrained coefficients that the sensitivity to experimental bounds gets too diluted at higher scales, so that the 95% HPDI interval for $|C_i|$ touches the prior’s edges, and consequently a bound on the scale cannot be obtained. RGE-induced effects are particularly relevant for coefficients such as C_G , which without RGE is mainly constrained by top-quark observables,¹⁶ or C_W , mainly constrained by EW observables, while including

¹⁶The C_G coefficient can also be strongly constrained using multijet production [146, 147] not present in our data set. As shown in those studies, the largest sensitivity to this operator comes from $\mathcal{O}(1/\Lambda^4)$ effects, while linear effects provide limited information.

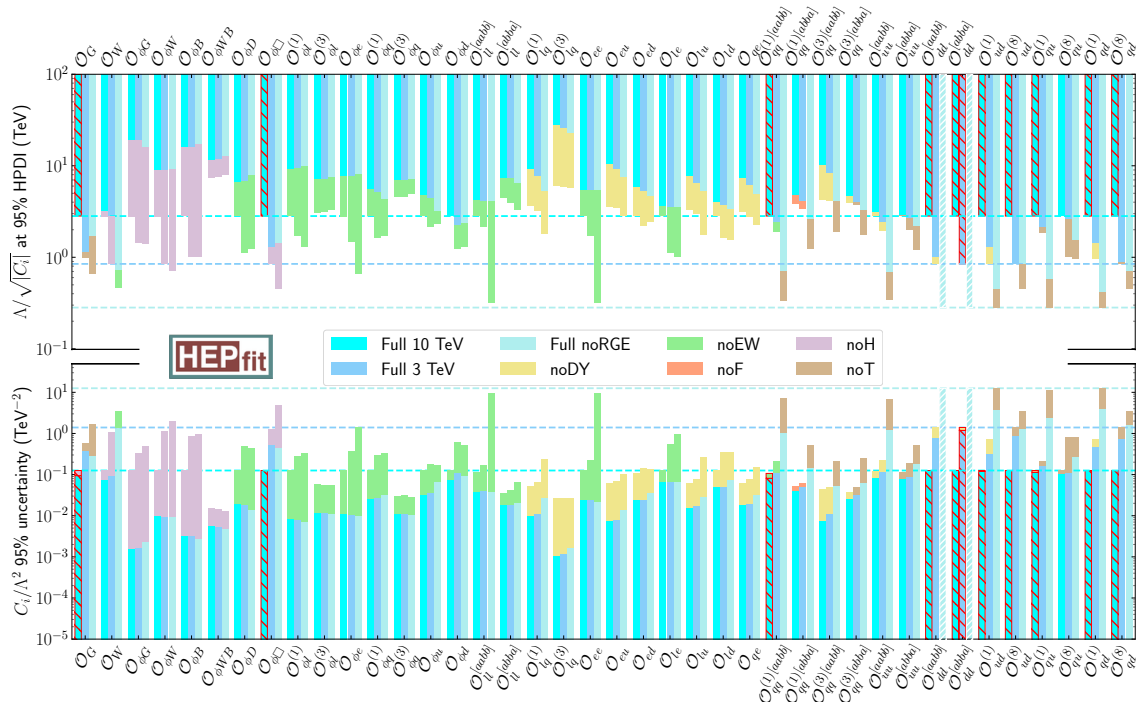


Figure 1. Results from individual fits in the $U(3)^5$ flavour symmetric SMEFT. For each coefficient C_i , the top panel shows the scale of NP allowed by the data at 95% probability (normalized by the square root of the maximum of the 95% HPDI interval for $|C_i|$). The bottom panel shows the width of the 95% probability range divided by two. Both panels show results for the three cases 1) $\Lambda = 10$ TeV with RGE, 2) $\Lambda = 3$ TeV with RGE, and 3) $\Lambda = 1$ TeV with no RGE. Furthermore, in each case we also include results obtained removing the most constraining data set for that particular coefficient (see Table 7). The color code is as explained in the legend. The horizontal lines indicate the maximum value allowed for each Wilson coefficient in the fit, corresponding to the perturbativity limit 4π (see Section 3.1), for the different values chosen for the NP scale Λ . The cases in which the 95% HPDI interval touches the prior’s edges, indicated in red in Table 7, are hatched with red diagonal lines. When the posterior distribution of a coefficient is completely flat the 95% HPDI interval is hatched with diagonal white lines.

RGE both get stronger constraints from Higgs-boson observables. This is also illustrated in Fig. 1, based on Table 7. In the lower panel, we report the half width of the 95% HPDI interval for $|C_i|/\Lambda^2$ for the three cases 1) $\Lambda = 10$ TeV with RGE, 2) $\Lambda = 3$ TeV with RGE, and 3) $\Lambda = 1$ TeV without RGE, both in the full fit (i.e. including all observables) and excluding the most constraining set of observables (using the color code explained in the figure). To guide the eye, we also draw the $4\pi/\Lambda^2$ perturbativity bound as a horizontal dashed line. The cases in which the 95% HPDI interval touches the prior’s edges, indicated in red in Table 7, are hatched with red diagonal lines. When the posterior is flat since the processes considered cannot bound the corresponding coefficient, the 95% HPDI interval is hatched with diagonal white lines. Thus, ranges touching the perturbativity line but solid or hatched in red can be refined by improving the precision of the measurements already included in the fit, while ranges hatched with diagonal white lines can only be improved by

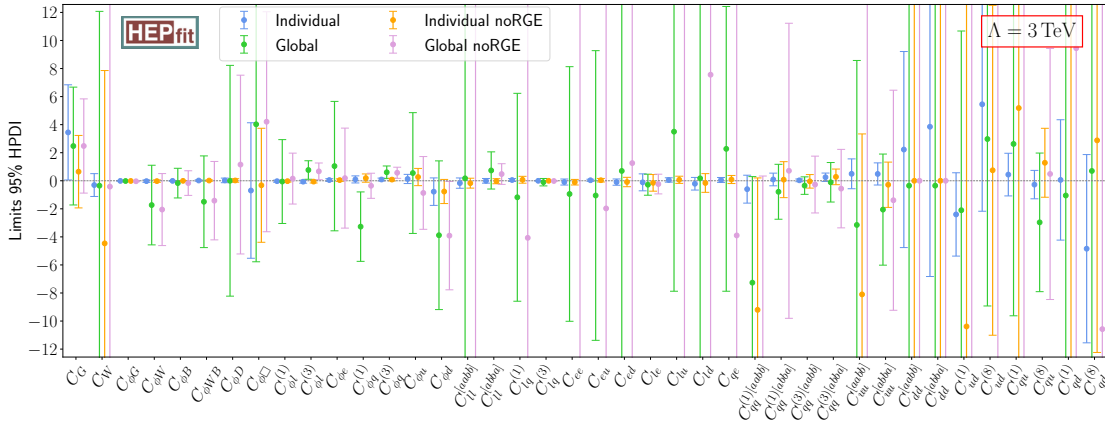


Figure 3. Comparison of individual and marginalised constraints from the global fit with $U(3)^5$ flavour symmetry assumption. The scale of NP has been set to $\Lambda = 3$ TeV. The limits shown correspond to the 95% HPDI. Results are presented for both individual and global fits, with and without the RGE effects (the latter also adjusted to a value of $\Lambda = 3$ TeV for this comparison), following the colour scheme indicated in the legend.

global one due to mutual strong correlations, we would like to emphasise that this implies that a lower effective NP scale $\Lambda/\sqrt{|C_i|}$ with respect to the one indicated by individual fits is viable only for those UV completions that incorporate the phenomenologically required correlations. Conversely, we note that taking into account the theory prior imposing perturbativity on the Wilson coefficients actually tightens many bounds. Table 8 shows that several limits on $\Lambda/\sqrt{|C_i|}$ at 10 TeV now exceed those at 3 TeV. In particular, although correlations with other operators substantially weaken the global-fit constraints on $C_{\phi B}$ and $C_{lq}^{(3)}$, restricting the allowed ranges of the correlated C_i/Λ^2 coefficients ensures that the bounds on $\Lambda/\sqrt{|C_{\phi B}|}$ and $\Lambda/\sqrt{|C_{lq}^{(3)}|}$ remain comparably strong at 10 TeV.

4.2 Results for the $U(2)^5$ flavour symmetric SMEFT

The results of the individual fits for the $U(2)^5$ flavour symmetric SMEFT in the UP basis are reported in Table 9 and in Figures 4-7, which have the same structure as Table 7 and Figure 1 discussed in Section 4.1 for the $U(3)^5$ case, to which we refer. The limits on $\Lambda/\sqrt{|C_i|}$ are also summarised in Figure 8, where we only show the coefficients that can be constrained individually within the perturbative regime in the case of $\Lambda = 3$ TeV. Furthermore, a comparison between the case of the UP and DOWN bases is summarised in Table 10 and Figure 9 for the case of those coefficients that are affected by the choice of flavour basis. Finally, the global fit results are shown in Table 11 and Figures 10 and 11 where we show the results for the case of $\Lambda = 10$ TeV.

The main points highlighted in the case of $U(3)^5$ still hold for $U(2)^5$, but there are several important new considerations that we discuss in the following. The first and most important one is that flavour observables play a crucial role in constraining many of the new coefficients appearing in the $U(2)^5$ case, consequently pushing the effective scale of

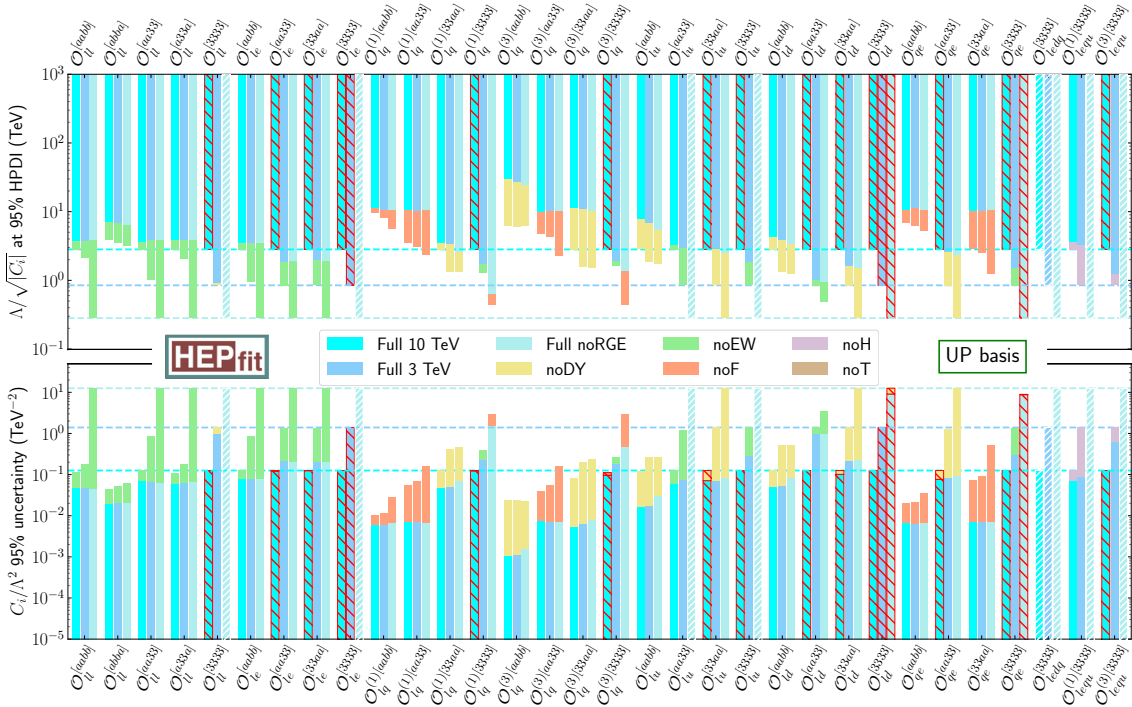


Figure 5. Same as Figure 4 but for the four-fermion operators that contain at least one leptonic field and one left-handed field.

HPDI interval of $[-0.30, 0.85]$ corresponding to a bound on $\Lambda/\sqrt{|C_{\phi G}|}$ of 10.5 TeV, to be compared with the bound of 19 TeV obtained in the individual fit (see Table 9). A similar phenomenon occurs for other pairs of coefficients, such as $C_{e\phi}^{[33]}$ and $C_{lequ}^{(1)[3333]}$, with a correlation coefficient of 0.91 and $C_{lequ}^{(1)[3333]}$ hitting the perturbativity limit; $C_{d\phi}^{[33]}$ and $C_{quqd}^{(1)[3333]}$, with a correlation coefficient of -0.91 and $C_{quqd}^{(1)[3333]}$ hitting the perturbativity limit; $C_{dB}^{[33]}$ and $C_{dW}^{[33]}$, with a correlation coefficient of 0.99, and $C_{dW}^{[33]}$ hitting the perturbativity limit; $C_{ll}^{[aabb]}$ and $C_{ee}^{[aabb]}$, with a correlation coefficient of -0.82 and both coefficients hitting the perturbativity limit. Another pair of strongly correlated coefficients is given by $C_{\phi e}^{[33]}$ and $C_{\phi e}^{[aa]}$, with a correlation coefficient of 0.84. Concerning four fermion operators, one faces more complex interference patterns involving several coefficients. For example, the coefficient $C_{qq}^{(3)[aabb]}$ is strongly correlated with $C_{lq}^{(3)[aabb]}$ which is in turn strongly correlated with $C_{lq}^{(3)[33aa]}$, with correlation coefficients of 0.93 and 0.85, respectively. Therefore, a large set of four fermions operators cannot be constrained in the global fit with current data.

A direct comparison between the global fit results in the $U(2)^5$ and $U(3)^5$ flavour-symmetric scenarios can be made by examining the last column of Tables 11 and 8. We have already discussed how certain dipole interactions involving the bottom quark ($C_{dB,dW,dG}^{[33]}$), which are absent under the $U(3)^5$ assumption, receive strong constraints from flavour observables in the $U(2)^5$ framework. On the other hand, when comparing the global bounds on operators such as $C_{\phi q}^{(1)}$ and $C_{\phi q}^{(3)}$, which modify the neutral and charged current couplings

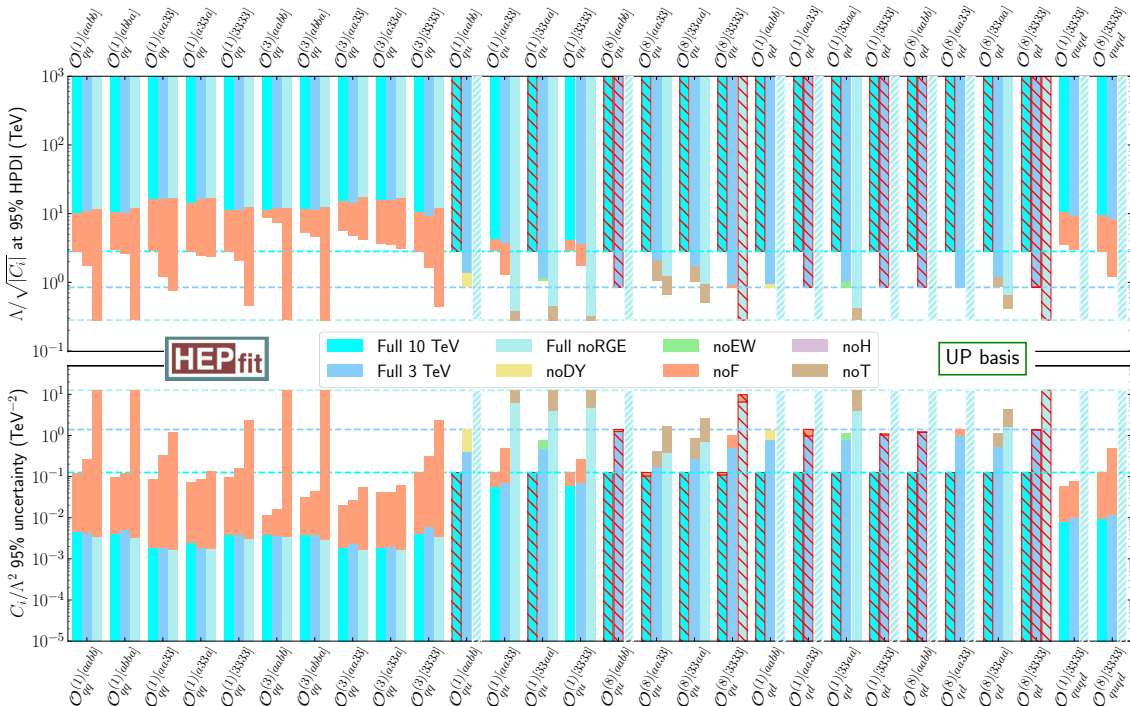


Figure 6. Same as Figure 4 but for the four-fermion operators that contain only quark fields and at least one left-handed field.

of left-handed quarks, we find that the $U(2)^5$ symmetry still offers significant protection against flavour constraints, yielding bounds comparable to those in the $U(3)^5$ scenario. However, this does not hold for individual fits. In particular, interactions involving the left-handed third-generation quarks are more strongly constrained by flavour observables, while those involving the light generations remain primarily constrained by electroweak data.¹⁷

Similar conclusions can be derived by looking at lepton-quark left-handed operators, where the separation of the third and first two families in the $U(2)^5$ also helps to identify the leading source of the bound in the $U(3)^5$ -symmetric case. For both the $C_{lq}^{(1),(3)}$ operators, this comes from the entries involving only the first two quark families, where Drell-Yan at high energies still seems to be the leading constraint. Unfortunately, the lack of constraints for many of the interactions in the $U(2)^5$ global fit does not allow to derive further information from the comparison with the $U(3)^5$ case.

As a final point, we note from Figures 10 and 11 that, similarly to the $U(3)^5$ case, the individual bounds are significantly weakened in the global case. Given the current precision of experimental measurements and theoretical predictions, constraining the most

¹⁷Interestingly, and as also pointed out in other studies, for the right-handed interactions with the top-quark, $C_{\phi u}^{[33]}$, the strongest individual bound comes from electroweak precision observables as a result of mixing between this operator and the custodial symmetry breaking operator $C_{\phi D}$ [149] (see also [150]). A similar effect is induced by the left-handed counterpart $C_{\phi q}^{(1)[33]}$, making electroweak bounds comparable to the flavour ones in this case (see Table 9).

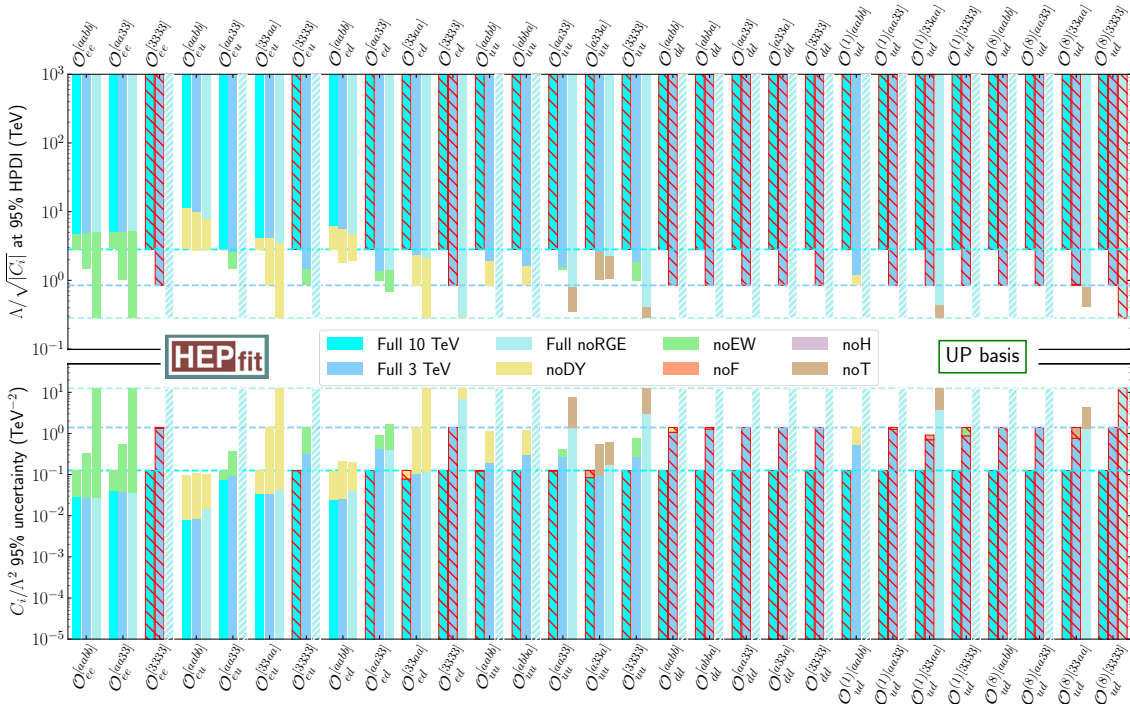


Figure 7. Same as Figure 4 but for the four-fermion operators that contain only right-handed fields.

general $U(2)^5$ -flavour-symmetric SMEFT becomes challenging for NP scales that ensure a reliable perturbative expansion, such as $\Lambda = 10$ TeV. Nevertheless, as previously noted, the presence of strong correlations between the coefficients does not prevent us from obtaining meaningful constraints on many of them when restricting to the perturbative regime.

5 Conclusions

The increasing accuracy reached in both experimental measurements and theoretical predictions for a large spectrum of observables over a broad range of scales allows to explore NP within the consistent and systematic framework of the SMEFT. This framework provides a powerful and model-independent approach to probe the reach of indirect NP searches at energies beyond the EW scale.

In this paper we have presented a comprehensive study aimed at assessing our capability to indirectly probe NP beyond the EW scale via a state-of-the-art global analysis of the dimension-6 SMEFT that still assumes lepton and baryon number conservation and no additional CP-violation beyond the SM. We have considered a broad set of observables including EW, Drell-Yan, top-quark, Higgs-boson, and key flavour measurements adopted for the unitarity triangle analysis as well as FCNC channels sensitive to NP. We have fitted the SMEFT Wilson coefficients together with floating SM and hadronic parameters, by comparing the measurements of such observables to the corresponding predictions in the SMEFT at linear order and with LO RGE of the Wilson coefficients. We investigated



Figure 8. Summary of individual lower bounds on the effective NP scale in the $U(2)^5$ flavour symmetric SMEFT obtained for $\Lambda = 3$ TeV in the UP basis.

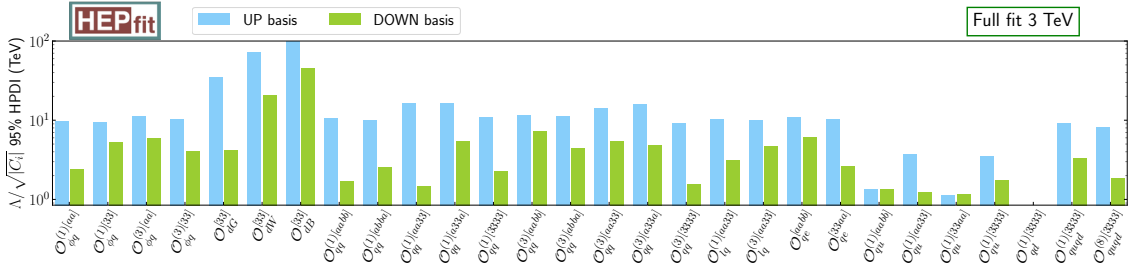


Figure 9. Comparison of the individual lower bounds on the effective NP scale in the $U(2)^5$ flavour symmetric SMEFT obtained for $\Lambda = 3$ TeV in the UP and DOWN basis. Only the operators constrained mostly from flavour observables are shown. The numerical values are also shown in Tab. 10.

two benchmark flavour symmetry scenarios: $U(3)^5$ and $U(2)^5$. Furthermore, in order to assess the extent to which current data constrain new physics at different energy scales, we have explored two representative benchmark values for the NP scale: $\Lambda = 3$, and 10 TeV including full RGE, and also compared them with results obtained without RGE (using

illustrated in Figure 8 and Figures 10-11.

In the $U(3)^5$ -symmetric case, the constraints on individual Wilson coefficients translate into lower bounds on the effective NP scale $\Lambda/\sqrt{|C_i|}$ reaching values up to ~ 25 TeV, particularly when RGE effects are included. We observe that the running of SMEFT operators plays a crucial role in tightening constraints for operators such as \mathcal{O}_G and \mathcal{O}_W , which gain sensitivity through mixing into observables in the Higgs and EW sectors. In global fits – where all relevant Wilson coefficients are varied simultaneously under the assumed flavour symmetry – strong correlations among them tend to relax many of the individual bounds. For instance, large correlations arise among several bosonic and four-fermion operators. Nevertheless, meaningful bounds persist: $\Lambda/\sqrt{|C_{\phi G}|} \gtrsim 14$ TeV and $\Lambda/\sqrt{|C_{lq}^{(3)}|} \gtrsim 5$ TeV, while other coefficients yield bounds in the 2–3 TeV range. These findings indicate that generic strongly-coupled $U(3)^5$ -symmetric NP scenarios are pushed above the TeV scale, ensuring the internal consistency of the SMEFT expansion. Conversely, weakly-coupled UV completions may still reside near the TeV scale, though in such cases the SMEFT description must be applied with care, particularly for high- p_T observables where EFT validity can break down.

In the $U(2)^5$ case, the orientation in flavour space becomes relevant, and the inclusion of flavour observables has a decisive impact on the analysis. In this study, we considered two complementary cases: one in which NP effects are introduced in the basis where the up-quark Yukawa matrix is diagonal – the UP basis – and another where NP effects are defined in the basis with diagonal down-quark Yukawas, the DOWN basis. In both cases, flavour misalignment stems from the left-handed quark sector, while the right-handed quarks can always be aligned with the direction of flavour-diagonal Yukawa couplings. In the lepton sector, the charged-lepton flavours can also always be rotated such that their Yukawa interactions are flavour diagonal.

Focusing on the UP basis, we find that several operators – such as $C_{dB}^{[33]}$, $C_{dW}^{[33]}$, and $C_{dG}^{[33]}$ – are strongly constrained by $B \rightarrow X_s \gamma$, with effective NP scales reaching several tens of TeV. Four-fermion operators, including various $C_{qq}^{(1),(3)}$ flavour configurations, are tightly constrained by meson mixing, and operators like $C_{qe}^{[33aa]}$ and $C_{qe}^{[aabb]}$ by rare decays such as $B_s \rightarrow \mu^+ \mu^-$. In global fits, the interplay of correlations once again leads to the saturation of perturbativity priors for certain coefficients; nevertheless, non-trivial bounds are retained for their correlated partners. For instance, the strong correlation between $C_{\phi G}$ and $C_{uG}^{[33]}$ still permits a meaningful constraint on $C_{\phi G}$, even when $C_{uG}^{[33]}$ approaches its prior limit. A comprehensive picture of the individual lower bounds derived in the $U(2)^5$ case within the UP basis is summarised in Figure 8 and a corresponding comparison of individual and marginalised constraints from the global fit is highlighted in Figures 10 and 11. Finally, in Figure 9, we compare the constraints on the set of operators that are sensitive to the choice of flavour basis – UP versus DOWN – for a reference NP scale of $\Lambda = 3$ TeV. The operators shown are those whose bounds are primarily driven by flavour observables and are therefore most affected by the basis-dependent treatment of third-generation quarks.

Comparing the $U(3)^5$ -symmetric case with the one of $U(2)^5$ in the UP basis, we note that several operators absent under $U(3)^5$ – notably the dipole interactions involving the

bottom quark, $\mathcal{O}_{dB}^{[33]}$, $\mathcal{O}_{dW}^{[33]}$, and $\mathcal{O}_{dG}^{[33]}$ — receive strong constraints in the $U(2)^5$ scenario due to the inclusion of flavour observables. This highlights the increased sensitivity to third-generation-specific operators once the full flavour symmetry is relaxed. On the other hand, for operators such as $\mathcal{O}_{\phi q}^{(1)}$ and $\mathcal{O}_{\phi q}^{(3)}$, which modify the neutral and charged currents of left-handed quarks, we find that the $U(2)^5$ symmetry still provides significant protection from flavour constraints. The resulting global bounds are comparable to those obtained in the $U(3)^5$ limit. However, the picture changes when examining individual coefficients: interactions involving third-generation left-handed quarks become more sensitive to flavour constraints, while those involving the light generations remain predominantly constrained by EW precision data. A similar pattern emerges in the case of lepton-quark interactions, particularly for the $\mathcal{O}_{lq}^{(1)}$ and $\mathcal{O}_{lq}^{(3)}$ operators. In the $U(3)^5$ case, the leading bounds are driven by contributions involving only the first two quark generations, with high-energy Drell-Yan processes providing the dominant constraints. In the $U(2)^5$ scenario, the separation between the third and first two generations helps isolate the origin of these bounds. However, the limited sensitivity of the $U(2)^5$ global fit to many operators hinders a more granular comparison with the $U(3)^5$ scenario. This limitation underscores the need for an expanded set of precision observables — particularly in the flavour sector — as well as improved experimental measurements in relation to EW, Higgs and top-quark physics.

Finally, in Figure 9 we provide a direct inspection of flavour constraints in relation to the choice of flavour basis. For instance, in the DOWN basis, where the third generation is aligned with the down-quark Yukawa couplings, the contributions of dipole operators like $\mathcal{O}_{dB}^{[33]}$ to flavour-changing b -quark processes are suppressed, leading to significantly weaker bounds — by nearly two orders of magnitude in some cases. Despite this suppression, flavour observables remain the primary source of constraints on these operators. This trend holds for most of the operators shown in Figure 9, where bounds in the DOWN basis are systematically weaker than in the UP basis. Notable exceptions are the $\mathcal{O}_{\phi q}^{(1)}$ and $\mathcal{O}_{\phi q}^{(3)}$ operators, for which electroweak precision observables continue to impose strong and largely basis-independent limits.

In summary, this analysis represents a significant advance in quantifying the indirect sensitivity of current data to physics beyond the SM within the SMEFT framework. Overall, our results underscore the interplay and complementarity of different classes of observables in constraining simultaneously SM and SMEFT parameters, and highlight the importance of continued progress in both theoretical precision and experimental accuracy to probe NP up to multi-TeV scales.

To conclude, one of the key takeaways of this work is the crucial role played by flavour assumptions in the SMEFT framework. Relaxing the $U(3)^5$ ansatz to a $U(2)^5$ structure introduces a greater number of SMEFT Wilson coefficients, and we have shown to what extent this weakens the constraints achievable in a global analysis. Looking ahead, and with the prospect of more data from current and future collider and low-energy experiments, we aim to further expand the spectrum of observables and to explore scenarios with different flavour assumptions, such as minimal flavour violation.

Acknowledgements

V.M. is grateful to Marcel Vos for insightful discussions during their joint work. He also thanks Antonio Jaques Costa for valuable advice on several experimental measurements. We thank P. Stangl for useful comments on the manuscript. The work of J.B. has been partially funded by the FEDER/Junta de Andalucía project grant P18-FRJ-3735, MICIU/AEI/10.13039/501100011033 and FEDER/UE (grant PID2022-139466NB-C21). The work of V.M. is supported by the MICIU through a Beatriz Galindo Junior grant (BG24/00038), the European Research Council (ERC) under the European Union’s Horizon 2020 research and innovation programme (Grant agreement No. 949451) and a Royal Society University Research Fellowship through grant URF/R1/201553. The work of L.R. is supported in part by the U.S. Department of Energy under grant DE-SC0010102 and by INFN through a Foreign Visiting Scientist Fellowship. This work was supported in part by the European Union - Next Generation EU under italian MUR grant PRIN-2022-RXEZCJ. L.S. and M.V. acknowledge support from the project “Exploring New Physics” funded by INFN.

A Relations between SMEFT operators under different flavour assumptions

In this appendix we present the defining relations of the $U(3)^5$ and $U(2)^5$ flavour-symmetric scenarios introduced in Section 2.1. Starting from the complete set of Wilson coefficients of the SMEFT, we specify the constraints imposed by the assumptions of the NP respecting the two flavour symmetries at the scale where the UV theory is matched with the effective field theory.

A.1 $U(3)^5$ flavour symmetric SMEFT

In this scenario, NP is assumed to be flavour-blind. The set of SMEFT bosonic interactions is unaffected by this assumption. For the fermionic Wilson coefficients the following identities are satisfied, with the left-handed side of each expression referring to the general SMEFT case, and the right-handed side introduces the notation we follow for the $U(3)^5$ -symmetric interactions:

$$\begin{aligned}
C_{e\phi}^{[pr]} &= C_{u\phi}^{[pr]} = C_{d\phi}^{[pr]} = C_{eX}^{[pr]} = C_{uX}^{[pr]} = C_{dX}^{[pr]} = C_{\phi ud}^{[pr]} = 0, \\
C_{\phi l}^{(1),(3)[pr]} &= C_{\phi l}^{(1),(3)} \delta_{pr}, & C_{\phi q}^{(1),(3)[pr]} &= C_{\phi q}^{(1),(3)} \delta_{pr}, \\
C_{\phi e}^{[pr]} &= C_{\phi e} \delta_{pr}, & C_{\phi u}^{[pr]} &= C_{\phi u} \delta_{pr}, & C_{\phi d}^{[pr]} &= C_{\phi d} \delta_{pr}, \\
C_{ll}^{[prst]} &= C_{ll}^{[aabb]} \delta_{pr} \delta_{st} + C_{ll}^{[abba]} \delta_{pt} \delta_{rs}, \\
C_{qq}^{(1),(3)[prst]} &= C_{qq}^{(1),(3)[aabb]} \delta_{pr} \delta_{st} + C_{qq}^{(1),(3)[abba]} \delta_{pt} \delta_{rs}, \\
C_{lq}^{(1),(3)[prst]} &= C_{lq}^{(1),(3)} \delta_{pr} \delta_{st}, & C_{ee}^{[prst]} &= C_{ee} \delta_{pr} \delta_{st}, \\
C_{uu}^{[prst]} &= C_{uu}^{[aabb]} \delta_{pr} \delta_{st} + C_{uu}^{[abba]} \delta_{pt} \delta_{rs}, \\
C_{dd}^{[prst]} &= C_{dd}^{[aabb]} \delta_{pr} \delta_{st} + C_{dd}^{[abba]} \delta_{pt} \delta_{rs}, \\
C_{eu}^{[prst]} &= C_{eu} \delta_{pr} \delta_{st}, & C_{ed}^{[prst]} &= C_{ed} \delta_{pr} \delta_{st}, & C_{ud}^{(1),(8)[prst]} &= C_{ud}^{(1),(8)} \delta_{pr} \delta_{st}, \\
C_{le}^{[prst]} &= C_{le} \delta_{pr} \delta_{st}, & C_{lu}^{[prst]} &= C_{lu} \delta_{pr} \delta_{st}, & C_{ld}^{[prst]} &= C_{ld} \delta_{pr} \delta_{st}, \\
C_{qe}^{[prst]} &= C_{qe} \delta_{pr} \delta_{st}, & C_{qu}^{(1),(8)[prst]} &= C_{qu}^{(1),(8)} \delta_{pr} \delta_{st}, & C_{qd}^{(1),(8)[prst]} &= C_{qd}^{(1),(8)} \delta_{pr} \delta_{st}, \\
C_{quqd}^{(1),(8)[prst]} &= C_{lequ}^{(1),(3)[prst]} = C_{ledq}^{[prst]} = 0.
\end{aligned} \tag{A.1}$$

A.2 $U(2)^5$ flavour symmetric SMEFT

In the $U(2)^5$ -symmetric scenario there are a total of 124 independent Wilson coefficients. The relations between the general SMEFT fermionic Wilson coefficients and the $U(2)^5$ -symmetric ones is given below in eq. (A.2). As in the previous case, the right-handed side of the expressions sets the notation we employ to refer to the independent degrees of freedom in this scenario. Note that, as emphasised in Section 2.1, this $U(2)^5$ limit is only

completely determined upon specifying the direction in flavour space that defines the third family.

$$\begin{aligned}
C_{\psi_R\phi}^{[pr]} &= C_{\psi_R\phi}^{[33]} \delta_{p3} \delta_{r3} \quad \text{for } \psi_R = e, u, d, \\
C_{\psi_RX}^{[pr]} &= C_{\psi_RX}^{[33]} \delta_{p3} \delta_{r3} \quad \text{for } \psi_R = e, u, d, \\
C_{\phi\psi_L}^{(1),(3)[pr]} &= C_{\phi\psi_L}^{(1),(3)[33]} \delta_{p3} \delta_{r3} + C_{\phi\psi_L}^{(1),(3)[aa]} \delta_{pr} (\delta_{p1} + \delta_{p2}) \quad \text{for } \psi_L = l, q, \\
C_{\phi\psi_R}^{[pr]} &= C_{\phi\psi_R}^{[33]} \delta_{p3} \delta_{r3} + C_{\phi\psi_R}^{[aa]} \delta_{pr} (\delta_{p1} + \delta_{p2}) \quad \text{for } \psi_R = e, u, d, \\
C_{\phi ud}^{[pr]} &= C_{\phi ud}^{[33]} \delta_{p3} \delta_{r3}, \\
C_{ll}^{[prst]} &= C_{ll}^{[3333]} \delta_{p3} \delta_{r3} \delta_{s3} \delta_{t3} + C_{ll}^{[aa33]} \delta_{pr} (\delta_{p1} + \delta_{p2}) \delta_{s3} \delta_{t3} + C_{ll}^{[a33a]} \delta_{pt} (\delta_{p1} + \delta_{p2}) \delta_{r3} \delta_{s3} + \\
&\quad C_{ll}^{[aabb]} \delta_{pr} \delta_{st} (\delta_{p1} + \delta_{p2}) (\delta_{s1} + \delta_{s2}) + C_{ll}^{[abba]} \delta_{pt} \delta_{rs} (\delta_{p1} + \delta_{p2}) (\delta_{s1} + \delta_{s2}), \\
C_{qq}^{(1),(3)[prst]} &= C_{qq}^{(1),(3)[3333]} \delta_{p3} \delta_{r3} \delta_{s3} \delta_{t3} + C_{qq}^{(1),(3)[aa33]} \delta_{pr} (\delta_{p1} + \delta_{p2}) \delta_{s3} \delta_{t3} + \\
&\quad C_{qq}^{(1),(3)[a33a]} \delta_{pt} (\delta_{p1} + \delta_{p2}) \delta_{r3} \delta_{s3} + C_{qq}^{(1),(3)[aabb]} \delta_{pr} \delta_{st} (\delta_{p1} + \delta_{p2}) (\delta_{s1} + \delta_{s2}) + \\
&\quad C_{qq}^{(1),(3)[abba]} \delta_{pt} \delta_{rs} (\delta_{p1} + \delta_{p2}) (\delta_{s1} + \delta_{s2}), \\
C_{lq}^{(1),(3)[prst]} &= C_{lq}^{(1),(3)[3333]} \delta_{p3} \delta_{r3} \delta_{s3} \delta_{t3} + C_{lq}^{(1),(3)[aa33]} \delta_{pr} (\delta_{p1} + \delta_{p2}) \delta_{s3} \delta_{t3} + \\
&\quad C_{lq}^{(1),(3)[33aa]} \delta_{st} (\delta_{s1} + \delta_{s2}) \delta_{p3} \delta_{r3} + C_{lq}^{(1),(3)[aabb]} \delta_{pr} \delta_{st} (\delta_{p1} + \delta_{p2}) (\delta_{s1} + \delta_{s2}), \\
C_{ee}^{[prst]} &= C_{ee}^{[3333]} \delta_{p3} \delta_{r3} \delta_{s3} \delta_{t3} + C_{ee}^{[aa33]} \delta_{pr} (\delta_{p1} + \delta_{p2}) \delta_{s3} \delta_{t3} + \\
&\quad C_{ee}^{[aabb]} \delta_{pr} \delta_{st} (\delta_{p1} + \delta_{p2}) (\delta_{s1} + \delta_{s2}), \\
C_{uu}^{[prst]} &= C_{uu}^{[3333]} \delta_{p3} \delta_{r3} \delta_{s3} \delta_{t3} + C_{uu}^{[aa33]} \delta_{pr} (\delta_{p1} + \delta_{p2}) \delta_{s3} \delta_{t3} + \\
&\quad C_{uu}^{[a33a]} \delta_{pt} (\delta_{p1} + \delta_{p2}) \delta_{r3} \delta_{s3} + C_{uu}^{[aabb]} \delta_{pr} \delta_{st} (\delta_{p1} + \delta_{p2}) (\delta_{s1} + \delta_{s2}) + \\
&\quad C_{uu}^{[abba]} \delta_{pt} \delta_{rs} (\delta_{p1} + \delta_{p2}) (\delta_{s1} + \delta_{s2}), \\
C_{dd}^{[prst]} &= C_{dd}^{[3333]} \delta_{p3} \delta_{r3} \delta_{s3} \delta_{t3} + C_{dd}^{[aa33]} \delta_{pr} (\delta_{p1} + \delta_{p2}) \delta_{s3} \delta_{t3} + \\
&\quad C_{dd}^{[a33a]} \delta_{pt} (\delta_{p1} + \delta_{p2}) \delta_{r3} \delta_{s3} + C_{dd}^{[aabb]} \delta_{pr} \delta_{st} (\delta_{p1} + \delta_{p2}) (\delta_{s1} + \delta_{s2}) + \\
&\quad C_{dd}^{[abba]} \delta_{pt} \delta_{rs} (\delta_{p1} + \delta_{p2}) (\delta_{s1} + \delta_{s2}), \\
C_{eu}^{[prst]} &= C_{eu}^{[3333]} \delta_{p3} \delta_{r3} \delta_{s3} \delta_{t3} + C_{eu}^{[aa33]} \delta_{pr} (\delta_{p1} + \delta_{p2}) \delta_{s3} \delta_{t3} + \\
&\quad C_{eu}^{[33aa]} \delta_{st} (\delta_{s1} + \delta_{s2}) \delta_{p3} \delta_{r3} + C_{eu}^{[aabb]} \delta_{pr} \delta_{st} (\delta_{p1} + \delta_{p2}) (\delta_{s1} + \delta_{s2}), \\
C_{ed}^{[prst]} &= C_{ed}^{[3333]} \delta_{p3} \delta_{r3} \delta_{s3} \delta_{t3} + C_{ed}^{[aa33]} \delta_{pr} (\delta_{p1} + \delta_{p2}) \delta_{s3} \delta_{t3} + \\
&\quad C_{ed}^{[33aa]} \delta_{st} (\delta_{s1} + \delta_{s2}) \delta_{p3} \delta_{r3} + C_{ed}^{[aabb]} \delta_{pr} \delta_{st} (\delta_{p1} + \delta_{p2}) (\delta_{s1} + \delta_{s2}), \\
C_{ud}^{(1),(8)[prst]} &= C_{ud}^{(1),(8)[3333]} \delta_{p3} \delta_{r3} \delta_{s3} \delta_{t3} + C_{ud}^{(1),(8)[aa33]} \delta_{pr} (\delta_{p1} + \delta_{p2}) \delta_{s3} \delta_{t3} + \\
&\quad C_{ud}^{(1),(8)[33aa]} \delta_{st} (\delta_{s1} + \delta_{s2}) \delta_{p3} \delta_{r3} + C_{ud}^{(1),(8)[aabb]} \delta_{pr} \delta_{st} (\delta_{p1} + \delta_{p2}) (\delta_{s1} + \delta_{s2}), \\
C_{le}^{[prst]} &= C_{le}^{[3333]} \delta_{p3} \delta_{r3} \delta_{s3} \delta_{t3} + C_{le}^{[aa33]} \delta_{pr} (\delta_{p1} + \delta_{p2}) \delta_{s3} \delta_{t3} + \\
&\quad C_{le}^{[33aa]} \delta_{p3} \delta_{r3} (\delta_{s1} + \delta_{s2}) \delta_{st} + C_{le}^{[aabb]} \delta_{pr} \delta_{st} (\delta_{p1} + \delta_{p2}) (\delta_{s1} + \delta_{s2}), \\
C_{lu}^{[prst]} &= C_{lu}^{[3333]} \delta_{p3} \delta_{r3} \delta_{s3} \delta_{t3} + C_{lu}^{[aa33]} \delta_{pr} (\delta_{p1} + \delta_{p2}) \delta_{s3} \delta_{t3} +
\end{aligned} \tag{A.2}$$

$$\begin{aligned}
& C_{lu}^{[33aa]} \delta_{p3} \delta_{r3} (\delta_{s1} + \delta_{s2}) \delta_{st} + C_{lu}^{[aabb]} \delta_{pr} \delta_{st} (\delta_{p1} + \delta_{p2}) (\delta_{s1} + \delta_{s2}), \\
C_{ld}^{[prst]} &= C_{ld}^{[3333]} \delta_{p3} \delta_{r3} \delta_{s3} \delta_{t3} + C_{ld}^{[aa33]} \delta_{pr} (\delta_{p1} + \delta_{p2}) \delta_{s3} \delta_{t3} + \\
& C_{ld}^{[33aa]} \delta_{p3} \delta_{r3} (\delta_{s1} + \delta_{s2}) \delta_{st} + C_{ld}^{[aabb]} \delta_{pr} \delta_{st} (\delta_{p1} + \delta_{p2}) (\delta_{s1} + \delta_{s2}), \\
C_{qe}^{[prst]} &= C_{qe}^{[3333]} \delta_{p3} \delta_{r3} \delta_{s3} \delta_{t3} + C_{qe}^{[aa33]} \delta_{pr} (\delta_{p1} + \delta_{p2}) \delta_{s3} \delta_{t3} + \\
& C_{qe}^{[33aa]} \delta_{p3} \delta_{r3} (\delta_{s1} + \delta_{s2}) \delta_{st} + C_{qe}^{[aabb]} \delta_{pr} \delta_{st} (\delta_{p1} + \delta_{p2}) (\delta_{s1} + \delta_{s2}), \\
C_{qu}^{(1),(8)[prst]} &= C_{qu}^{(1),(8)[3333]} \delta_{p3} \delta_{r3} \delta_{s3} \delta_{t3} + C_{qu}^{(1),(8)[aa33]} \delta_{pr} (\delta_{p1} + \delta_{p2}) \delta_{s3} \delta_{t3} + \\
& C_{qu}^{(1),(8)[33aa]} \delta_{st} (\delta_{s1} + \delta_{s2}) \delta_{p3} \delta_{r3} + C_{qu}^{(1),(8)[aabb]} \delta_{pr} \delta_{st} (\delta_{p1} + \delta_{p2}) (\delta_{s1} + \delta_{s2}), \\
C_{qd}^{(1),(8)[prst]} &= C_{qd}^{(1),(8)[3333]} \delta_{p3} \delta_{r3} \delta_{s3} \delta_{t3} + C_{qd}^{(1),(8)[aa33]} \delta_{pr} (\delta_{p1} + \delta_{p2}) \delta_{s3} \delta_{t3} + \\
& C_{qd}^{(1),(8)[33aa]} \delta_{st} (\delta_{s1} + \delta_{s2}) \delta_{p3} \delta_{r3} + C_{qd}^{(1),(8)[aabb]} \delta_{pr} \delta_{st} (\delta_{p1} + \delta_{p2}) (\delta_{s1} + \delta_{s2}), \\
C_{quqd}^{(1),(8)[prst]} &= C_{quqd}^{(1),(8)[3333]} \delta_{p3} \delta_{r3} \delta_{s3} \delta_{t3}, \\
C_{lequ}^{(1),(3)[prst]} &= C_{lequ}^{(1),(3)[3333]} \delta_{p3} \delta_{r3} \delta_{s3} \delta_{t3}, \\
C_{ledq}^{[prst]} &= C_{ledq}^{[3333]} \delta_{p3} \delta_{r3} \delta_{s3} \delta_{t3}.
\end{aligned}$$

B Tables of results

In this appendix we collect a series of tables with the numerical results presented in the figures discussed in the main text, as well as some supplementary results. We report both the 68% HPDI interval for the Wilson coefficients at the different scales considered in the study, as well as the bound on $\Lambda/\sqrt{|C_i|}$ in units of TeV obtained from the maximum of the 95% HPDI interval for $|C_i|$. As indicated in the main text, in some cases the 68% or 95% HPDI (from which the bound on $\Lambda/\sqrt{|C_i|}$ is obtained) touches the edges of the prior dictated by perturbativity. These cases are indicated in the tables in red colour. On the other hand, in those cases where the posterior distribution of a given coefficient does not allow to set a bound, we indicate that using a dash.

B.1 Results for the $U(3)^5$ flavour symmetric SMEFT

Table 7: Results of the individual fits for the $U(3)^5$ flavour symmetric SMEFT. For each coefficient, we report the 68% HPDI interval, the bound on $\Lambda/\sqrt{|C_i|}$ in units of TeV obtained taking the maximum of the 95% HPDI interval for $|C_i|$, and the set of observables that give the strongest constraint (EW stands for Electroweak, F for Flavour, H for Higgs, T for top, and DY for Drell-Yan). Results are shown with RG evolution for $\Lambda = 10$ TeV, for $\Lambda = 3$ TeV and without RG evolution. A dash denotes that no bound can be set from that particular fit. The meaning of the colour code is discussed in the text.

	10 TeV			3 TeV			1 TeV - noRGE		
	C_i	$\Lambda/\sqrt{ C_i }$	Obs	C_i	$\Lambda/\sqrt{ C_i }$	Obs	C_i	$\Lambda/\sqrt{ C_i }$	Obs
$C_{\phi\Box}$	–	–	–	-0.7 ± 3.0	1.2	H	-0.02 ± 0.29	1.3	H
$C_{\phi D}$	0.3 ± 1.1	6.4	EW	0.040 ± 0.090	6.5	EW	0.0024 ± 0.0072	7.7	EW
$C_{\phi G}$	-0.112 ± 0.084	19.0	H	-0.0102 ± 0.0084	18.5	H	-0.0017 ± 0.0012	15.8	H
$C_{\phi B}$	-0.10 ± 0.17	15.4	H	-0.008 ± 0.015	15.6	H	-0.0008 ± 0.0014	17.0	H
$C_{\phi W}$	-0.33 ± 0.52	8.7	H	-0.028 ± 0.047	8.8	H	-0.0029 ± 0.0051	8.8	H
$C_{\phi WB}$	0.19 ± 0.29	11.3	H	0.018 ± 0.025	11.6	H	0.0017 ± 0.0025	12.2	H
C_G	10.3 ± 4.7	–	H/T	3.5 ± 1.8	1.1	T	0.07 ± 0.15	1.7	T
C_W	-2.2 ± 3.8	3.2	H	-0.25 ± 0.43	2.9	H	-0.50 ± 0.70	0.7	EW
$C_{\phi l}^{(1)}$	-0.33 ± 0.45	9.1	EW	-0.030 ± 0.039	9.2	EW	-0.0029 ± 0.0039	9.8	EW
$C_{\phi l}^{(3)}$	-0.67 ± 0.64	7.3	EW	-0.058 ± 0.056	7.3	EW	-0.0061 ± 0.0058	7.6	EW
$C_{\phi e}$	0.62 ± 0.59	7.6	EW	0.052 ± 0.051	7.7	EW	0.0053 ± 0.0053	8.2	EW
$C_{\phi q}^{(1)}$	0.8 ± 1.4	5.4	EW	0.10 ± 0.13	5.0	EW	0.022 ± 0.017	4.2	EW
$C_{\phi q}^{(3)}$	1.01 ± 0.58	6.7	EW	0.086 ± 0.052	6.8	EW	0.0090 ± 0.0058	7.0	EW
$C_{\phi u}$	1.3 ± 1.7	4.7	EW	0.13 ± 0.18	4.3	EW	0.033 ± 0.035	3.1	EW

Table 7: Results of the individual fits for the $U(3)^5$ flavour symmetric SMEFT. For each coefficient, we report the 68% HPDI interval, the bound on $\Lambda/\sqrt{|C_i|}$ in units of TeV obtained taking the maximum of the 95% HPDI interval for $|C_i|$, and the set of observables that give the strongest constraint (EW stands for Electroweak, F for Flavour, H for Higgs, T for top, and DY for Drell-Yan). Results are shown with RG evolution for $\Lambda = 10$ TeV, for $\Lambda = 3$ TeV and without RG evolution. A dash denotes that no bound can be set from that particular fit. The meaning of the colour code is discussed in the text.

	10 TeV			3 TeV			1 TeV - noRGE		
	C_i	$\Lambda/\sqrt{ C_i }$	Obs	C_i	$\Lambda/\sqrt{ C_i }$	Obs	C_i	$\Lambda/\sqrt{ C_i }$	Obs
$C_{\phi d}$	-10.3 ± 4.4	-	EW	-0.83 ± 0.51	2.2	EW	-0.087 ± 0.051	2.3	EW
$C_{ll}^{[aabb]}$	-1.7 ± 2.1	4.2	EW	-0.15 ± 0.19	4.1	EW	-0.019 ± 0.021	4.0	EW
$C_{ll}^{[abba]}$	-0.01 ± 0.96	7.3	EW	-0.005 ± 0.091	6.9	EW	-0.004 ± 0.010	6.3	EW
$C_{qq}^{(1)[aabb]}$	-5.8 ± 4.6	2.7	EW	-0.62 ± 0.54	2.3	EW	-1.00 ± 0.55	0.7	T
$C_{qq}^{(1)[abba]}$	0.3 ± 2.2	4.7	F/DY	0.09 ± 0.23	4.0	F/DY	0.005 ± 0.075	2.5	T
$C_{qq}^{(3)[aabb]}$	0.21 ± 0.40	9.9	DY	0.034 ± 0.050	8.3	DY	-0.005 ± 0.029	4.1	T
$C_{qq}^{(3)[abba]}$	2.0 ± 1.4	4.5	DY/T	0.25 ± 0.16	4.0	T/DY	0.031 ± 0.034	3.3	T
$C_{lq}^{(1)}$	0.23 ± 0.51	8.8	DY	0.055 ± 0.054	7.4	DY	0.007 ± 0.014	5.3	DY
$C_{lq}^{(3)}$	-0.028 ± 0.058	26.7	DY	-0.0035 ± 0.0055	24.9	DY	-0.00034 ± 0.00087	21.9	DY
C_{ee}	-1.0 ± 1.3	5.3	EW	-0.10 ± 0.12	5.3	EW	-0.011 ± 0.012	5.4	EW
$C_{uu}^{[aabb]}$	2.2 ± 4.4	3.1	DY	0.47 ± 0.56	2.4	DY	-0.87 ± 0.65	0.7	T
$C_{uu}^{[abba]}$	4.2 ± 4.1	2.8	T	0.51 ± 0.40	2.6	T	-0.032 ± 0.092	2.1	T
$C_{dd}^{[aabb]}$	-	-	-	2.4 ± 3.7	1.0	DY	-	-	-
$C_{dd}^{[abba]}$	-	-	-	3.9 ± 6.0	-	DY	-	-	-
C_{eu}	0.17 ± 0.41	10.2	DY	0.036 ± 0.038	9.0	DY	0.0046 ± 0.0076	7.3	DY
$C_{ed}^{(1)}$	-0.5 ± 1.3	5.7	DY	-0.10 ± 0.12	5.2	DY	-0.010 ± 0.020	4.6	DY
$C_{ud}^{(8)}$	-8.2 ± 6.8	-	EW	-2.4 ± 1.6	1.3	DY	-1.3 ± 2.0	0.4	T
$C_{ud}^{(8)}$	6.3 ± 8.8	-	T	5.5 ± 4.1	0.8	T	0.05 ± 0.70	0.8	T
C_{le}	-1.0 ± 3.6	3.5	EW	-0.11 ± 0.31	3.5	EW	-0.014 ± 0.035	3.5	EW
C_{lu}	0.12 ± 0.85	7.4	DY	0.050 ± 0.084	6.4	DY	0.008 ± 0.015	5.2	DY
C_{ld}	-1.3 ± 2.7	3.9	DY	-0.21 ± 0.24	3.7	DY	-0.020 ± 0.039	3.3	DY
C_{qe}	0.0 ± 1.0	7.0	DY	0.057 ± 0.095	6.2	DY	0.008 ± 0.017	4.8	T
$C_{qu}^{(1)}$	1.1 ± 6.3	2.7	DY/EW	0.40 ± 0.80	2.1	DY/EW	0.5 ± 1.3	0.6	T
$C_{qu}^{(8)}$	-2.6 ± 5.4	2.7	T	-0.27 ± 0.53	2.6	T	0.15 ± 0.14	1.5	T
$C_{qd}^{(1)}$	5.5 ± 9.5	-	EW	-0.1 ± 2.3	1.4	DY/EW	-1.5 ± 2.1	0.4	T
$C_{qd}^{(8)}$	-6.8 ± 8.2	-	T	-4.8 ± 3.5	0.9	T	0.28 ± 0.88	0.7	T

Table 8: Results of the individual fits compared to those from the global fit for the $U(3)^5$ flavour symmetric SMEFT. For each coefficient, we report the 68% HPDI interval and the bound on $\Lambda/\sqrt{|C_i|}$ in units of TeV obtained taking the maximum of the 95% HPDI interval for $|C_i|$. Results are shown with RG evolution for $\Lambda = 3$ TeV and $\Lambda = 10$ TeV.

	Individual 3 TeV		Global 3 TeV		Individual 10 TeV		Global 10 TeV	
	C_i	$\Lambda/\sqrt{ C_i }$	C_i	$\Lambda/\sqrt{ C_i }$	C_i	$\Lambda/\sqrt{ C_i }$	C_i	$\Lambda/\sqrt{ C_i }$
$C_{\phi\Box}$	-0.7 ± 3.0	1.2	4.6 ± 5.3	0.8	-	-	-	-
$C_{\phi D}$	0.040 ± 0.090	6.5	-0.2 ± 4.4	1.0	0.3 ± 1.1	6.4	-	-
$C_{\phi G}$	-0.0102 ± 0.0084	18.5	0.016 ± 0.013	14.1	-0.112 ± 0.084	19.0	-0.14 ± 0.10	16.8
$C_{\phi B}$	-0.008 ± 0.015	15.6	-0.17 ± 0.56	2.7	-0.10 ± 0.17	15.4	-0.5 ± 2.4	4.6
$C_{\phi W}$	-0.028 ± 0.047	8.8	-1.8 ± 1.5	1.4	-0.33 ± 0.52	8.7	-12.0 ± 2.8	-
$C_{\phi WB}$	0.018 ± 0.025	11.6	-1.4 ± 1.7	1.4	0.19 ± 0.29	11.3	-7.3 ± 4.9	-
C_G	3.5 ± 1.8	1.1	2.4 ± 2.1	1.2	10.3 ± 4.7	-	8.2 ± 6.8	-
C_W	-0.25 ± 0.43	2.9	-1.1 ± 7.0	0.8	-2.2 ± 3.8	3.2	-	-
$C_{\phi l}^{(1)}$	-0.030 ± 0.039	9.2	-0.2 ± 1.5	1.7	-0.33 ± 0.45	9.1	2.9 ± 3.3	3.5
$C_{\phi l}^{(3)}$	-0.058 ± 0.056	7.3	0.80 ± 0.35	2.5	-0.67 ± 0.64	7.3	4.8 ± 3.0	3.1
$C_{\phi e}$	0.052 ± 0.051	7.7	1.0 ± 2.5	1.3	0.62 ± 0.59	7.6	9.8 ± 5.1	-
$C_{\phi q}^{(1)}$	0.10 ± 0.13	5.0	-3.5 ± 1.3	1.2	0.8 ± 1.4	5.4	-3.1 ± 4.7	2.9
$C_{\phi q}^{(3)}$	0.086 ± 0.052	6.8	0.61 ± 0.25	2.9	1.01 ± 0.58	6.7	6.4 ± 2.1	3.1
$C_{\phi u}$	0.13 ± 0.18	4.3	1.0 ± 2.3	1.3	1.3 ± 1.7	4.7	-6.8 ± 7.2	-
$C_{\phi d}$	-0.83 ± 0.51	2.2	-3.9 ± 3.0	1.0	-10.3 ± 4.4	-	-8.2 ± 6.8	-
$C_{ll}^{[aabb]}$	-0.15 ± 0.19	4.1	-	-	-1.7 ± 2.1	4.2	-	-
$C_{ll}^{[abba]}$	-0.005 ± 0.091	6.9	0.82 ± 0.74	2.1	-0.01 ± 0.96	7.3	2.1 ± 3.4	3.6
$C_{qq}^{(1)[aabb]}$	-0.62 ± 0.54	2.3	-11.2 ± 3.8	-	-5.8 ± 4.6	2.7	-8.6 ± 6.5	-
$C_{qq}^{(1)[abba]}$	0.09 ± 0.23	4.0	-0.8 ± 1.0	1.8	0.3 ± 2.2	4.7	5.3 ± 3.4	2.9
$C_{qq}^{(3)[aabb]}$	0.034 ± 0.050	8.3	-0.36 ± 0.33	3.0	0.21 ± 0.40	9.9	-0.5 ± 3.1	3.8
$C_{qq}^{(3)[abba]}$	0.25 ± 0.16	4.0	-0.24 ± 0.74	2.4	2.0 ± 1.4	4.5	3.7 ± 2.5	3.3

Table 8: Results of the individual fits compared to those from the global fit for the $U(3)^5$ flavour symmetric SMEFT. For each coefficient, we report the 68% HPDI interval and the bound on $\Lambda/\sqrt{|C_i|}$ in units of TeV obtained taking the maximum of the 95% HPDI interval for $|C_i|$. Results are shown with RG evolution for $\Lambda = 3$ TeV and $\Lambda = 10$ TeV.

	Individual 3 TeV		Global 3 TeV		Individual 10 TeV		Global 10 TeV	
	C_i	$\Lambda/\sqrt{ C_i }$	C_i	$\Lambda/\sqrt{ C_i }$	C_i	$\Lambda/\sqrt{ C_i }$	C_i	$\Lambda/\sqrt{ C_i }$
$C_{lq}^{(1)}$	0.055 ± 0.054	7.4	-2.5 ± 4.3	1.0	0.23 ± 0.51	8.8	-3.7 ± 4.9	2.7
$C_{lq}^{(3)}$	-0.0035 ± 0.0055	24.9	-0.10 ± 0.14	4.9	-0.028 ± 0.058	26.7	-0.03 ± 0.51	9.7
C_{ee}	-0.10 ± 0.12	5.3	-4.6 ± 5.4	0.9	-1.0 ± 1.3	5.3	-2.9 ± 6.8	2.7
$C_{uu}^{[aabb]}$	0.47 ± 0.56	2.4	-9.5 ± 5.6	–	2.2 ± 4.4	3.1	–	–
$C_{uu}^{[abba]}$	0.51 ± 0.40	2.6	-2.3 ± 2.0	1.2	4.2 ± 4.1	2.8	-8.9 ± 6.1	–
$C_{dd}^{[aabb]}$	2.4 ± 3.7	1.0	–	–	–	–	–	–
$C_{dd}^{[abba]}$	3.9 ± 6.0	–	–	–	–	–	–	–
C_{eu}	0.036 ± 0.038	9.0	0.9 ± 6.1	0.9	0.17 ± 0.41	10.2	$2.6 \pm 8.2.5$	–
C_{ed}	-0.10 ± 0.12	5.2	6.5 ± 7.2	–	-0.5 ± 1.3	5.7	–	–
$C_{ud}^{(1)}$	-2.4 ± 1.6	1.3	-7.9 ± 7.2	–	-8.2 ± 6.8	–	–	–
$C_{ud}^{(8)}$	5.5 ± 4.1	0.8	8.4 ± 6.6	–	6.3 ± 8.8	–	–	–
C_{le}	-0.11 ± 0.31	3.5	-0.28 ± 0.39	2.9	-1.0 ± 3.6	3.5	-1.7 ± 3.6	3.3
C_{lu}	0.050 ± 0.084	6.4	5.3 ± 6.7	0.8	0.12 ± 0.85	7.4	–	–
C_{ld}	-0.21 ± 0.24	3.7	–	–	-1.3 ± 2.7	3.9	–	–
C_{qe}	0.057 ± 0.095	6.2	1.6 ± 5.8	0.8	0.0 ± 1.0	7.0	–	–
$C_{qu}^{(1)}$	0.40 ± 0.80	2.1	6.8 ± 7.2	–	1.1 ± 6.3	2.7	–	–
$C_{qu}^{(8)}$	-0.27 ± 0.53	2.6	-3.7 ± 2.6	1.0	-2.6 ± 5.4	2.7	-1.8 ± 7.0	2.7
$C_{qd}^{(1)}$	-0.1 ± 2.3	1.4	–	–	5.5 ± 9.5	–	–	–
$C_{qd}^{(8)}$	-4.8 ± 3.5	0.9	–	–	-6.8 ± 8.2	–	–	–

B.2 Results for the $U(2)^5$ flavour symmetric SMEFT

Table 9: Same as Table 7, presenting the results of the individual fits for the $U(2)^5$ flavour symmetric SMEFT in the UP basis.

	10 TeV			3 TeV			1 TeV - noRGE		
	C_i	$\Lambda/\sqrt{ C_i }$	Obs	C_i	$\Lambda/\sqrt{ C_i }$	Obs	C_i	$\Lambda/\sqrt{ C_i }$	Obs
$C_{\phi\Box}$	–	–	–	-0.7 ± 3.0	1.2	H	-0.02 ± 0.29	1.3	H
$C_{\phi D}$	0.3 ± 1.1	6.4	EW	0.040 ± 0.090	6.5	EW	0.0024 ± 0.0072	7.7	EW
$C_{\phi G}$	-0.112 ± 0.084	19.0	H	-0.0102 ± 0.0084	18.5	H	-0.0017 ± 0.0012	15.8	H
$C_{\phi B}$	-0.10 ± 0.17	15.4	H	-0.008 ± 0.015	15.6	H	-0.0008 ± 0.0014	17.0	H
$C_{\phi W}$	-0.33 ± 0.52	8.7	H	-0.028 ± 0.047	8.8	H	-0.0029 ± 0.0051	8.8	H
$C_{\phi WB}$	0.19 ± 0.29	11.3	H	0.018 ± 0.025	11.6	H	0.0017 ± 0.0025	12.2	H
C_G	10.3 ± 4.7	–	H/T	3.5 ± 1.8	1.1	T	0.07 ± 0.15	1.7	T
C_W	-2.2 ± 3.8	3.2	H	-0.25 ± 0.43	2.9	H	-0.50 ± 0.70	0.7	EW
$C_{\phi l}^{(1)[33]}$	0.4 ± 1.8	5.0	EW	0.03 ± 0.16	5.1	EW	0.002 ± 0.015	5.4	EW
$C_{\phi l}^{(1)[aa]}$	-0.43 ± 0.47	8.5	EW	-0.040 ± 0.043	8.6	EW	-0.0034 ± 0.0040	9.2	EW
$C_{\phi l}^{(3)[33]}$	1.2 ± 1.5	4.9	EW	0.10 ± 0.14	4.9	EW	0.010 ± 0.014	5.1	EW
$C_{\phi l}^{(3)[aa]}$	-0.82 ± 0.61	7.1	EW	-0.071 ± 0.054	7.2	EW	-0.0072 ± 0.0058	7.4	EW
$C_{\phi l}^{[33]}$	-1.7 ± 2.0	4.3	EW	-0.15 ± 0.17	4.3	EW	-0.015 ± 0.017	4.6	EW
$C_{\phi e}^{[aa]}$	0.76 ± 0.62	7.2	EW	0.063 ± 0.053	7.3	EW	0.0067 ± 0.0054	7.6	EW
$C_{\phi q}^{(1)[33]}$	0.32 ± 0.40	9.4	F	0.029 ± 0.036	9.5	F	0.0029 ± 0.0037	9.9	F
$C_{\phi q}^{(1)[aa]}$	-0.28 ± 0.41	9.5	F	-0.022 ± 0.037	9.5	F	-0.0024 ± 0.0036	10.2	F
$C_{\phi q}^{(3)[33]}$	0.27 ± 0.33	10.2	F	0.026 ± 0.030	10.1	F	0.0031 ± 0.0037	9.9	F
$C_{\phi q}^{(3)[aa]}$	0.15 ± 0.35	11.0	F	0.010 ± 0.030	11.1	F	0.0012 ± 0.0032	11.9	F
$C_{\phi u}^{[33]}$	0.8 ± 1.9	4.7	EW	0.10 ± 0.20	4.4	EW	0.586 ± 0.946	0.64	T
$C_{\phi u}^{[aa]}$	4.8 ± 4.3	2.8	EW	0.43 ± 0.37	2.8	EW	0.043 ± 0.036	3.0	EW
$C_{\phi d}^{[33]}$	-10.9 ± 4.2	–	EW	-2.0 ± 1.1	1.5	EW	-0.21 ± 0.10	1.6	EW
$C_{\phi d}^{[aa]}$	-8.8 ± 6.0	–	EW	-0.86 ± 0.78	1.9	EW	-0.080 ± 0.074	2.1	EW
$C_{\phi ud}^{[33]}$	–	–	–	4.6 ± 5.6	0.8	H	-8.9 ± 6.1	–	T
$C_{e\phi}^{[33]}$	0.20 ± 0.98	6.7	H	0.020 ± 0.086	6.7	H	0.0021 ± 0.0085	7.3	H
$C_{u\phi}^{[33]}$	–	–	–	5.3 ± 4.3	0.8	H	0.52 ± 0.41	0.9	H
$C_{d\phi}^{[33]}$	0.7 ± 1.0	6.1	H	0.080 ± 0.093	6.0	H	0.009 ± 0.012	5.5	H
C_{eB}	–	–	–	6.3 ± 8.1	–	H	1.6 ± 3.2	0.4	H

Table 9: Same as Table 7, presenting the results of the individual fits for the $U(2)^5$ flavour symmetric SMEFT in the UP basis.

	10 TeV			3 TeV			1 TeV - noRGE		
	C_i	$\Lambda/\sqrt{ C_i }$	Obs	C_i	$\Lambda/\sqrt{ C_i }$	Obs	C_i	$\Lambda/\sqrt{ C_i }$	Obs
$C_{uB}^{[33]}$	-0.7 ± 1.4	5.4	H	-0.10 ± 0.17	4.6	H	0.017 ± 0.048	2.9	H
$C_{dE}^{[33]}$	-0.0015 ± 0.0041	100.2	F	-0.00012 ± 0.00037	101.0	F	-0.000016 ± 0.000036	106.2	F
$C_{eW}^{[33]}$	-	-	-	0.4 ± 2.2	1.4	H	-3.3 ± 4.9	-	H
$C_{uW}^{[33]}$	-1.2 ± 2.2	4.2	H	-0.12 ± 0.26	3.8	H	-0.007 ± 0.073	2.6	H
$C_{dW}^{[33]}$	0.0032 ± 0.0078	72.4	F	0.00028 ± 0.00070	72.3	F	0.000027 ± 0.000068	76.8	F
$C_{uG}^{[33]}$	-1.9 ± 1.2	4.9	H	-0.27 ± 0.15	4.0	H	0.009 ± 0.033	3.7	H
$C_{dG}^{[33]}$	-0.014 ± 0.032	36.9	F	-0.0014 ± 0.0031	33.6	F	-0.00022 ± 0.00060	26.5	F
$C_{ll}^{[3333]}$	-	-	-	2.8 ± 4.6	0.9	DY	-	-	-
$C_{ll}^{[aa33]}$	-0.1 ± 3.7	3.7	EW	0.00 ± 0.32	3.8	EW	-0.002 ± 0.034	3.8	EW
$C_{ll}^{[a33a]}$	0.8 ± 3.2	3.7	EW	0.06 ± 0.29	3.8	EW	-0.003 ± 0.035	3.8	EW
$C_{ll}^{[aabb]}$	-2.5 ± 2.6	3.7	EW	-0.21 ± 0.23	3.7	EW	-0.026 ± 0.024	3.6	EW
$C_{ll}^{[abba]}$	-0.1 ± 1.0	6.8	EW	-0.005 ± 0.099	6.7	EW	-0.003 ± 0.011	6.3	EW
$C_{qq}^{(1)[3333]}$	-0.45 ± 0.23	10.7	F	-0.043 ± 0.020	10.7	F	-0.0036 ± 0.0018	11.9	F
$C_{qq}^{(1)[aa33]}$	0.235 ± 0.099	15.1	F	0.0192 ± 0.0096	15.4	F	0.00182 ± 0.00088	16.8	F
$C_{qq}^{(1)[a33a]}$	0.214 ± 0.096	15.5	F	0.0188 ± 0.0096	15.3	F	0.00178 ± 0.00086	17.0	F
$C_{qq}^{(1)[aabb]}$	-0.43 ± 0.22	10.2	F	-0.036 ± 0.018	11.2	F	-0.0035 ± 0.0016	12.2	F
$C_{qq}^{(1)[abba]}$	-0.47 ± 0.22	10.7	F	-0.036 ± 0.021	10.1	F	-0.0039 ± 0.0018	11.8	F
$C_{qq}^{(3)[3333]}$	-0.56 ± 0.23	10.2	F	-0.040 ± 0.020	10.4	F	-0.0038 ± 0.0018	11.9	F
$C_{qq}^{(3)[aa33]}$	0.22 ± 0.13	13.5	F	0.0207 ± 0.0096	15.1	F	0.00192 ± 0.00090	16.3	F
$C_{qq}^{(3)[a33a]}$	0.18 ± 0.11	15.7	F	0.0194 ± 0.0094	15.8	F	0.00192 ± 0.00096	16.7	F
$C_{qq}^{(3)[aabb]}$	-0.36 ± 0.21	11.5	F	-0.032 ± 0.019	11.2	F	-0.0038 ± 0.0018	12.0	F
$C_{qq}^{(3)[abba]}$	-0.40 ± 0.21	10.6	F	-0.036 ± 0.018	11.1	F	-0.0039 ± 0.0019	11.3	F
$C_{lq}^{(1)[3333]}$	-7.1 ± 7.1	-	EW	-0.9 ± 1.1	1.7	EW	-0.21 ± 0.24	1.2	F
$C_{lq}^{(1)[aa33]}$	-0.21 ± 0.38	10.1	F	-0.019 ± 0.035	10.1	F	-0.0021 ± 0.0036	10.3	F
$C_{lq}^{(1)[33aa]}$	3.6 ± 2.5	3.4	DY	0.33 ± 0.24	3.3	DY	0.076 ± 0.038	2.6	DY
$C_{lq}^{(1)[aabb]}$	0.17 ± 0.31	11.3	F	0.024 ± 0.030	10.4	F	0.0022 ± 0.0035	10.2	F
$C_{lq}^{(3)[3333]}$	8.2 ± 5.8	-	EW/DY	0.93 ± 0.91	1.8	EW	0.15 ± 0.24	1.3	F
$C_{lq}^{(3)[aa33]}$	-0.25 ± 0.39	9.7	F	-0.022 ± 0.034	10.0	F	-0.0023 ± 0.0038	10.0	F
$C_{lq}^{(3)[33aa]}$	-0.21 ± 0.29	11.1	DY	-0.018 ± 0.031	10.6	DY	-0.0022 ± 0.0042	9.8	DY
$C_{lq}^{(3)[aabb]}$	-0.011 ± 0.056	29.2	DY	-0.0016 ± 0.0053	27.1	DY	-0.00007 ± 0.00084	24.3	DY
$C_{ee}^{[3333]}$	-	-	-	7.2 ± 7.2	-	EW/DY	-	-	-
$C_{ee}^{[aa33]}$	0.0 ± 2.1	4.9	EW	0.01 ± 0.18	4.9	EW	-0.003 ± 0.019	4.9	EW
$C_{ee}^{[aabb]}$	-1.4 ± 1.5	4.8	EW	-0.13 ± 0.13	4.8	EW	-0.015 ± 0.014	4.8	EW
$C_{uu}^{[3333]}$	2.5 ± 8.1	-	EW	0.2 ± 1.3	1.8	EW	-2.912 ± 1.56	0.41	T
$C_{uu}^{[aa33]}$	6.8 ± 7.2	-	T	1.3 ± 1.3	1.5	EW	-0.17 ± 0.56	1.0	T
$C_{uu}^{[a33a]}$	6.3 ± 4.7	2.6	T	0.55 ± 0.44	2.5	T	0.014 ± 0.092	2.2	T
$C_{uu}^{[aabb]}$	1.6 ± 6.8	2.7	DY	0.72 ± 0.91	1.9	DY	-	-	-
$C_{uu}^{[abba]}$	2.5 ± 8.4	-	DY	1.0 ± 1.3	1.6	DY	-	-	-
$C_{dd}^{[3333]}$	-	-	-	-	-	-	-	-	-
$C_{dd}^{[aa33]}$	-	-	-	6.0 ± 8.1	-	EW/DY	-	-	-
$C_{dd}^{[a33a]}$	-	-	-	-	-	-	-	-	-
$C_{dd}^{[aabb]}$	-	-	-	3.9 ± 5.3	0.8	DY	-	-	-
$C_{dd}^{[abba]}$	-	-	-	4.2 ± 6.7	-	DY	-	-	-
$C_{eu}^{[3333]}$	-8.2 ± 6.8	-	EW	-1.3 ± 1.5	1.4	EW	-	-	-
$C_{eu}^{[aa33]}$	5.4 ± 4.0	2.8	EW	0.56 ± 0.44	2.5	EW	-	-	-
$C_{eu}^{[33aa]}$	2.7 ± 1.8	4.0	DY	0.24 ± 0.17	4.1	DY	0.041 ± 0.022	3.4	DY
$C_{eu}^{[aabb]}$	-0.02 ± 0.41	11.0	DY	0.021 ± 0.039	9.5	DY	-0.0013 ± 0.0077	7.9	DY
$C_{eu}^{[abba]}$	-	-	-	-	-	-	-4.8 ± 3.7	0.3	DY
$C_{ed}^{[3333]}$	-	-	-	-	-	-	-	-	-
$C_{ed}^{[aa33]}$	5.6 ± 9.5	-	EW	1.1 ± 2.0	1.3	EW	0.08 ± 0.22	1.4	EW
$C_{ed}^{[33aa]}$	-7.9 ± 4.7	-	DY	-0.73 ± 0.50	2.3	DY	-0.110 ± 0.061	2.1	DY
$C_{ed}^{[aabb]}$	0.0 ± 1.4	5.9	DY	-0.06 ± 0.12	5.4	DY	0.003 ± 0.021	4.8	DY
$C_{ud}^{(1)[3333]}$	-6.5 ± 8.3	-	EW	-10.9 ± 4.2	-	EW	-	-	-
$C_{ud}^{(1)[aa33]}$	-	-	-	-5.1 ± 6.8	-	DY	-	-	-
$C_{ud}^{(1)[33aa]}$	-7.4 ± 7.7	-	EW/T	-10.3 ± 3.7	-	EW	-1.5 ± 1.9	0.4	T
$C_{ud}^{(1)[aabb]}$	-6.0 ± 8.8	-	DY	-1.9 ± 2.6	1.1	DY	-	-	-
$C_{ud}^{(8)[3333]}$	-	-	-	-	-	-	5.5 ± 9.5	-	T
$C_{ud}^{(8)[aa33]}$	-	-	-	-	-	-	-	-	-
$C_{ud}^{(8)[33aa]}$	6.8 ± 8.3	-	T	5.2 ± 3.6	0.9	T	0.33 ± 0.71	0.8	T
$C_{ud}^{(8)[aabb]}$	-	-	-	-	-	-	-	-	-
$C_{le}^{[3333]}$	-	-	-	8.1 ± 6.9	-	DY	-	-	-
$C_{le}^{[aa33]}$	-4.2 ± 7.1	-	EW	-0.65 ± 0.98	1.9	EW	-0.08 ± 0.11	1.8	EW
$C_{le}^{[33aa]}$	-6.7 ± 7.7	-	EW	-0.55 ± 0.99	1.9	EW	-0.08 ± 0.11	1.8	EW
$C_{le}^{[aabb]}$	0.4 ± 4.2	3.3	EW	0.04 ± 0.38	3.4	EW	0.000 ± 0.041	3.4	EW

Table 9: Same as Table 7, presenting the results of the individual fits for the $U(2)^5$ flavour symmetric SMEFT in the UP basis.

	10 TeV			3 TeV			1 TeV - noRGE		
	C_i	$\Lambda/\sqrt{ C_i }$	Obs	C_i	$\Lambda/\sqrt{ C_i }$	Obs	C_i	$\Lambda/\sqrt{ C_i }$	Obs
$C_{lu}^{[3333]}$	2.5 ± 8.8	–	EW	0.3 ± 1.4	1.7	EW	–	–	–
$C_{[aa33]}^{[aa33]}$	-2.8 ± 3.3	3.3	EW	-0.32 ± 0.37	2.9	EW	–	–	–
$C_{[33aa]}^{[33aa]}$	5.7 ± 3.8	2.8	DY	0.49 ± 0.35	2.8	DY	0.083 ± 0.045	2.4	DY
$C_{[aabb]}^{[aabb]}$	-0.03 ± 0.89	7.4	DY	0.042 ± 0.084	6.6	DY	-0.002 ± 0.016	5.6	DY
$C_{[3333]}^{[3333]}$	–	–	–	–	–	–	-9.5 ± 5.3	–	DY
$C_{[aa33]}^{[aa33]}$	–	–	–	0.4 ± 4.6	1.0	EW	0.15 ± 0.53	0.9	EW
$C_{[33aa]}^{[33aa]}$	-9.8 ± 5.3	–	DY	-1.4 ± 1.1	1.6	DY	-0.23 ± 0.13	1.4	DY
$C_{[aabb]}^{[aabb]}$	-0.4 ± 2.7	4.1	DY	-0.14 ± 0.24	3.8	DY	0.000 ± 0.043	3.4	DY
$C_{[3333]}^{[3333]}$	7.7 ± 7.4	–	EW	1.1 ± 1.5	1.5	EW	8.2 ± 5.4	–	DY
$C_{[aa33]}^{[aa33]}$	6.9 ± 4.4	2.6	DY	0.62 ± 0.40	2.6	DY	0.091 ± 0.049	2.3	DY
$C_{[33aa]}^{[33aa]}$	0.22 ± 0.38	10.0	F	0.020 ± 0.035	9.9	F	0.0024 ± 0.0036	10.1	F
$C_{[aabb]}^{[aabb]}$	-0.23 ± 0.36	10.4	F	-0.015 ± 0.032	10.8	F	-0.0021 ± 0.0035	10.3	F
$C_{qu}^{(1)[3333]}$	0.3 ± 3.1	3.9	F	0.08 ± 0.36	3.4	F	4.77 ± 2.53	0.32	T
$C_{qu}^{(1)[aa33]}$	0.1 ± 2.9	4.2	F	0.02 ± 0.34	3.6	F	-1.1 ± 3.3	0.4	T
$C_{qu}^{(1)[33aa]}$	-7.0 ± 6.9	–	F	-2.5 ± 2.3	1.1	F	–	–	–
$C_{qu}^{(1)[aabb]}$	3.6 ± 9.1	–	DY	1.5 ± 1.9	1.3	DY	–	–	–
$C_{qu}^{(8)[3333]}$	-10.3 ± 4.7	–	F	-6.2 ± 2.5	0.9	F	-7.6 ± 2.5	–	T
$C_{qu}^{(8)[aa33]}$	6.8 ± 6.1	–	F/T	0.50 ± 0.78	2.1	T	0.32 ± 0.21	1.2	T
$C_{qu}^{(8)[33aa]}$	-5.8 ± 8.2	–	T	-0.6 ± 1.3	1.7	T	0.43 ± 0.36	–	T
$C_{qu}^{(8)[aabb]}$	–	–	–	-8.1 ± 6.7	–	–	–	–	–
$C_{qd}^{(1)[3333]}$	–	–	–	3.6 ± 4.4	0.9	F	–	–	–
$C_{qd}^{(1)[aa33]}$	–	–	–	–	–	–	–	–	–
$C_{qd}^{(1)[33aa]}$	–	–	–	-1.1 ± 3.6	1.1	EW	-1.65 ± 2.15	0.41	T
$C_{qd}^{(1)[aabb]}$	–	–	–	-0.9 ± 3.9	1.0	DY	–	–	–
$C_{qd}^{(8)[3333]}$	–	–	–	-1.2 ± 6.1	0.9	F	6.0 ± 9.0	–	T
$C_{qd}^{(8)[aa33]}$	–	–	–	–	–	–	–	–	–
$C_{qd}^{(8)[33aa]}$	–	–	–	-1.1 ± 2.7	1.1	T	0.85 ± 0.87	0.6	T
$C_{qd}^{(8)[aabb]}$	–	–	–	-3.6 ± 4.4	0.8	F	–	–	–
$C_{[3333]}^{[3333]}$	–	–	–	–	–	–	–	–	–
$C_{[leqq]}^{[leqq]}$	–	–	–	–	–	–	–	–	–
$C_{quqd}^{(1)[3333]}$	-0.10 ± 0.40	10.2	F	-0.014 ± 0.047	9.2	F	–	–	–
$C_{quqd}^{(8)[3333]}$	-0.16 ± 0.48	9.2	F	-0.020 ± 0.054	8.1	F	–	–	–
$C_{lequ}^{(1)[3333]}$	-1.2 ± 3.7	3.5	H	-0.10 ± 0.40	3.1	H	–	–	–
$C_{lequ}^{(3)[3333]}$	–	–	–	0.5 ± 2.9	1.2	H	–	–	–

Table 10: Results of the individual fits in the UP basis (first two columns) and in the DOWN basis (second two columns) for the $U(2)^5$ flavour symmetric SMEFT, limited to those coefficients that are mainly constrained by flavour observables. Results are presented for $\Lambda = 3$ TeV and under the same assumptions on HPDI used in previous tables for both coefficient and scale bounds.

	Full Fit UP		no Flavour UP		Full Fit DOWN		no Flavour DOWN	
	C_i	$\Lambda/\sqrt{ C_i }$	C_i	$\Lambda/\sqrt{ C_i }$	C_i	$\Lambda/\sqrt{ C_i }$	C_i	$\Lambda/\sqrt{ C_i }$
$C_{\phi q}^{(1)[33]}$	0.029 ± 0.036	9.5	0.08 ± 0.14	5.0	0.06 ± 0.14	5.1	0.08 ± 0.14	5.0
$C_{\phi q}^{(1)[aa]}$	-0.022 ± 0.037	9.5	0.46 ± 0.60	2.4	0.48 ± 0.56	2.4	0.38 ± 0.60	2.4
$C_{\phi q}^{(3)[33]}$	0.026 ± 0.030	10.1	0.21 ± 0.18	4.0	0.22 ± 0.17	4.0	0.20 ± 0.18	4.0
$C_{\phi q}^{(3)[aa]}$	0.010 ± 0.030	11.1	0.124 ± 0.066	6.0	0.134 ± 0.068	5.8	0.122 ± 0.069	5.9
$C_{dB}^{[33]}$	-0.00012 ± 0.00037	101.0	3.7 ± 5.1	0.8	1.3 ± 1.7	1.3	4.4 ± 5.1	0.8
$C_{dW}^{[33]}$	0.00028 ± 0.00070	72.3	0.44 ± 0.57	2.4	-0.0033 ± 0.0091	20.2	0.42 ± 0.56	2.4
$C_{dG}^{[33]}$	-0.0014 ± 0.0031	33.6	-2.3 ± 4.0	0.9	0.08 ± 0.22	4.2	-2.3 ± 3.9	1.0
$C_{qq}^{(1)[3333]}$	-0.043 ± 0.020	10.7	-0.65 ± 0.74	2.0	-0.40 ± 0.70	2.2	-0.66 ± 0.76	2.1
$C_{qq}^{(1)[aa33]}$	0.0192 ± 0.0096	15.4	-3.1 ± 1.6	1.2	-2.2 ± 1.1	1.4	-3.1 ± 1.5	1.2
$C_{qq}^{(1)[a33a]}$	0.0188 ± 0.0096	15.3	0.72 ± 0.41	2.4	0.14 ± 0.28	3.5	0.73 ± 0.42	2.4
$C_{qq}^{(1)[aabb]}$	-0.036 ± 0.018	11.2	0.7 ± 1.2	1.7	1.0 ± 1.1	1.7	0.6 ± 1.2	1.7
$C_{qq}^{(1)[abba]}$	-0.036 ± 0.021	10.1	0.24 ± 0.59	2.6	0.38 ± 0.58	2.5	0.23 ± 0.59	2.5
$C_{qq}^{(3)[3333]}$	-0.040 ± 0.020	10.4	1.0 ± 1.4	1.5	1.4 ± 1.2	1.5	0.6 ± 1.4	1.5
$C_{qq}^{(3)[aa33]}$	0.0207 ± 0.0096	15.1	0.13 ± 0.13	4.9	0.11 ± 0.12	5.2	0.15 ± 0.13	4.8
$C_{qq}^{(3)[a33a]}$	0.0194 ± 0.0094	15.8	0.33 ± 0.20	3.5	0.28 ± 0.17	3.8	0.32 ± 0.20	3.5
$C_{qq}^{(3)[aabb]}$	-0.032 ± 0.019	11.2	0.032 ± 0.078	6.9	0.031 ± 0.079	7.0	0.031 ± 0.079	7.0
$C_{qq}^{(3)[abba]}$	-0.036 ± 0.018	11.1	0.06 ± 0.20	4.5	0.06 ± 0.20	4.4	0.06 ± 0.20	4.4
$C_{lq}^{(1)[aa33]}$	-0.019 ± 0.035	10.1	0.28 ± 0.32	3.1	0.35 ± 0.30	3.2	0.33 ± 0.33	3.1
$C_{lq}^{(1)[aabb]}$	0.024 ± 0.030	10.4	0.035 ± 0.056	8.0	0.028 ± 0.055	8.0	0.030 ± 0.056	8.1
$C_{lq}^{(3)[aa33]}$	-0.022 ± 0.034	10.0	0.00 ± 0.25	4.2	0.02 ± 0.22	4.7	-0.01 ± 0.25	4.2
$C_{qe}^{[33aa]}$	0.020 ± 0.035	9.9	-0.58 ± 0.45	2.5	-0.59 ± 0.40	2.6	-0.55 ± 0.46	2.5

Table 10: Results of the individual fits in the UP basis (first two columns) and in the DOWN basis (second two columns) for the $U(2)^5$ flavour symmetric SMEFT, limited to those coefficients that are mainly constrained by flavour observables. Results are presented for $\Lambda = 3$ TeV and under the same assumptions on HPDI used in previous tables for both coefficient and scale bounds.

	Full Fit UP		no Flavour UP		Full Fit DOWN		no Flavour DOWN	
	C_i	$\Lambda/\sqrt{ C_i }$	C_i	$\Lambda/\sqrt{ C_i }$	C_i	$\Lambda/\sqrt{ C_i }$	C_i	$\Lambda/\sqrt{ C_i }$
$C_{[aabb]}^{[ae]}$	-0.015 ± 0.032	10.8	0.055 ± 0.099	6.0	0.06 ± 0.10	6.0	0.05 ± 0.10	6.0
$C_{[3333]}^{(1)[qu]}$	0.08 ± 0.36	3.4	0.7 ± 1.3	1.7	0.6 ± 1.2	1.7	0.7 ± 1.3	1.7
$C_{[aa33]}^{(1)[qu]}$	0.02 ± 0.34	3.6	1.0 ± 2.2	1.3	1.5 ± 2.3	1.2	1.1 ± 0.0	1.3
$C_{[3333]}^{(1)[qd]}$	3.6 ± 4.4	0.9	11.2 ± 3.9	0.8	11.2 ± 3.9	0.8	10.9 ± 4.2	0.8
$C_{[3333]}^{(1)[quqd]}$	-0.014 ± 0.047	9.2	0.31 ± 0.37	3.0	0.24 ± 0.29	3.3	0.31 ± 0.37	3.0
$C_{[quqd]}^{(8)[3333]}$	-0.020 ± 0.054	8.1	1.9 ± 2.3	1.2	0.7 ± 1.0	1.8	1.9 ± 2.3	1.2

Table 11: Results of the individual fits (first two columns) and of the global fit (second two columns) for the $U(2)^5$ flavour symmetric SMEFT. For each coefficient, we report the 68% HPDI interval and the bound on $\Lambda/\sqrt{|C_i|}$ in units of TeV obtained taking the maximum of the 95% HPDI interval for $|C_i|$. Results are shown with RG evolution for $\Lambda = 10$ TeV. All results are obtained in the UP basis.

	10 TeV Individual		10 TeV Global	
	C_i	$\Lambda/\sqrt{ C_i }$	C_i	$\Lambda/\sqrt{ C_i }$
$C_{\phi D}$	0.3 ± 1.1	6.4	–	–
$C_{\phi G}$	-0.112 ± 0.084	19.0	0.31 ± 0.30	10.5
$C_{\phi B}$	-0.10 ± 0.17	15.4	0.3 ± 2.0	5.1
$C_{\phi W}$	-0.33 ± 0.52	8.7	-6.5 ± 4.7	–
$C_{\phi WB}$	0.19 ± 0.29	11.3	-3.7 ± 4.8	2.7
C_G	10.3 ± 4.7	–	–	–
C_W	-2.2 ± 3.8	3.2	–	–
$C_{\phi l}^{(1)[33]}$	0.4 ± 1.8	5.0	1.2 ± 5.1	3.1
$C_{\phi l}^{(1)[aa]}$	-0.43 ± 0.47	8.5	4.0 ± 3.3	3.1
$C_{\phi l}^{(3)[33]}$	1.2 ± 1.5	4.9	3.8 ± 3.4	2.7
$C_{\phi l}^{(3)[aa]}$	-0.82 ± 0.61	7.1	3.2 ± 3.2	3.2
$C_{\phi e}^{[33]}$	-1.7 ± 2.0	4.3	3.0 ± 5.1	3.1
$C_{\phi e}^{[aa]}$	0.76 ± 0.62	7.2	6.4 ± 5.3	2.7
$C_{\phi q}^{(1)[33]}$	0.32 ± 0.40	9.4	1.6 ± 8.3	2.7
$C_{\phi q}^{(1)[aa]}$	-0.28 ± 0.41	9.5	-3.0 ± 7.6	2.7
$C_{\phi q}^{(3)[33]}$	0.27 ± 0.33	10.2	8.6 ± 6.4	–
$C_{\phi q}^{(3)[aa]}$	0.15 ± 0.35	11.0	6.2 ± 2.6	3.1
$C_{\phi u}^{[33]}$	0.8 ± 1.9	4.7	–	–
$C_{\phi u}^{[aa]}$	4.8 ± 4.3	2.8	-8 ± 7	–
$C_{\phi d}^{[33]}$	-10.9 ± 4.2	–	-8.1 ± 6.7	–
$C_{\phi d}^{[aa]}$	-8.8 ± 6.0	–	–	–
$C_{e\phi}^{[33]}$	0.20 ± 0.98	6.7	0.3 ± 2.4	4.5
$C_{d\phi}^{[33]}$	0.7 ± 1.0	6.1	5.5 ± 3.0	3.1
$C_{uB}^{[33]}$	-0.7 ± 1.4	5.4	–	–
$C_{dB}^{[33]}$	-0.0015 ± 0.0041	100.2	0 ± 4.3	3.5
$C_{uW}^{[33]}$	-1.2 ± 2.2	4.2	–	–
$C_{dW}^{[33]}$	0.0032 ± 0.0078	72.4	–	–
$C_{uG}^{[33]}$	-1.9 ± 1.2	4.9	–	–

Table 11: Results of the individual fits (first two columns) and of the global fit (second two columns) for the $U(2)^5$ flavour symmetric SMEFT. For each coefficient, we report the 68% HPDI interval and the bound on $\Lambda/\sqrt{|C_i|}$ in units of TeV obtained taking the maximum of the 95% HPDI interval for $|C_i|$. Results are shown with RG evolution for $\Lambda = 10$ TeV. All results are obtained in the UP basis.

	10 TeV Individual		10 TeV Global	
	C_i	$\Lambda/\sqrt{ C_i }$	C_i	$\Lambda/\sqrt{ C_i }$
$C_{dG}^{[33]}$	-0.014 ± 0.032	36.9	1.1 ± 0.9	6.6
$C_{ll}^{[aa33]}$	-0.1 ± 3.7	3.7	–	–
$C_{ll}^{[a33a]}$	0.8 ± 3.2	3.7	–	–
$C_{ll}^{[aabb]}$	-2.5 ± 2.6	3.7	–	–
$C_{ll}^{[abba]}$	-0.1 ± 1.0	6.8	-0.6 ± 3.3	3.8
$C_{qq}^{(1)[3333]}$	-0.45 ± 0.23	10.7	–	–
$C_{qq}^{(1)[aa33]}$	0.235 ± 0.099	15.1	–	–
$C_{qq}^{(1)[a33a]}$	0.214 ± 0.096	15.5	–	–
$C_{qq}^{(1)[aabb]}$	-0.43 ± 0.22	10.2	–	–
$C_{qq}^{(1)[abba]}$	-0.47 ± 0.22	10.7	–	–
$C_{qq}^{(3)[3333]}$	-0.56 ± 0.23	10.2	–	–
$C_{qq}^{(3)[aa33]}$	0.22 ± 0.13	13.5	-0.5 ± 3.2	4.2
$C_{qq}^{(3)[a33a]}$	0.18 ± 0.11	15.7	3.8 ± 4.2	2.8
$C_{qq}^{(3)[aabb]}$	-0.36 ± 0.21	11.5	–	–
$C_{qq}^{(3)[abba]}$	-0.40 ± 0.21	10.6	–	–
$C_{lq}^{(1)[3333]}$	-7.1 ± 7.1	–	–	–
$C_{lq}^{(1)[aa33]}$	-0.21 ± 0.38	10.1	-7.0 ± 8.1	–
$C_{lq}^{(1)[33aa]}$	3.6 ± 2.5	3.4	-2.6 ± 8.2	–
$C_{lq}^{(1)[aabb]}$	0.17 ± 0.31	11.3	-3.9 ± 4.6	2.8
$C_{lq}^{(3)[3333]}$	8.2 ± 5.8	–	–	–
$C_{lq}^{(3)[aa33]}$	-0.25 ± 0.39	9.7	5.6 ± 7.0	–
$C_{lq}^{(3)[33aa]}$	-0.21 ± 0.29	11.1	-0.2 ± 1.2	7.3
$C_{lq}^{(3)[aabb]}$	-0.011 ± 0.056	29.2	-0.1 ± 1.1	7.7
$C_{ee}^{[aa33]}$	0.0 ± 2.1	4.9	-2.0 ± 5.2	2.8
$C_{ee}^{[aabb]}$	-1.4 ± 1.5	4.8	-2.4 ± 5.1	3.2
$C_{uu}^{[3333]}$	2.5 ± 8.1	–	–	–
$C_{uu}^{[aa33]}$	6.8 ± 7.2	–	–	–
$C_{uu}^{[a33a]}$	6.3 ± 4.7	2.6	-1.9 ± 5.8	3.0
$C_{uu}^{[aabb]}$	1.6 ± 6.8	2.7	–	–
$C_{uu}^{[abba]}$	2.5 ± 8.4	–	–	–
$C_{eu}^{[3333]}$	-8.2 ± 6.8	–	–	–
$C_{eu}^{[aa33]}$	5.4 ± 4.0	2.8	0.9 ± 6.9	2.7
$C_{eu}^{[33aa]}$	2.7 ± 1.8	4.0	2.1 ± 5.4	2.8
$C_{eu}^{[aabb]}$	-0.02 ± 0.41	11.0	-1.5 ± 4.5	2.7
$C_{ed}^{[aa33]}$	5.6 ± 9.5	–	–	–
$C_{ed}^{[33aa]}$	-7.9 ± 4.7	–	–	–
$C_{ed}^{[aabb]}$	0.0 ± 1.4	5.9	–	–

Table 11: Results of the individual fits (first two columns) and of the global fit (second two columns) for the $U(2)^5$ flavour symmetric SMEFT. For each coefficient, we report the 68% HPDI interval and the bound on $\Lambda/\sqrt{|C_i|}$ in units of TeV obtained taking the maximum of the 95% HPDI interval for $|C_i|$. Results are shown with RG evolution for $\Lambda = 10$ TeV. All results are obtained in the UP basis.

	10 TeV Individual		10 TeV Global	
	C_i	$\Lambda/\sqrt{ C_i }$	C_i	$\Lambda/\sqrt{ C_i }$
$C_{ud}^{(1)[3333]}$	-6.5 ± 8.3	–	–	–
$C_{ud}^{(1)[33aa]}$	-7.4 ± 7.7	–	–	–
$C_{ud}^{(1)[aabb]}$	-6.0 ± 8.8	–	–	–
$C_{ud}^{(8)[33aa]}$	6.8 ± 8.3	–	–	–
$C_{le}^{[aa33]}$	-4.2 ± 7.1	–	–	–
$C_{le}^{[33aa]}$	-6.7 ± 7.7	–	–	–
$C_{le}^{[aabb]}$	0.4 ± 4.2	3.3	2.1 ± 4.8	3.2
$C_{lu}^{[3333]}$	2.5 ± 8.8	–	–	–
$C_{lu}^{[aa33]}$	-2.8 ± 3.3	3.3	–	–
$C_{lu}^{[33aa]}$	5.7 ± 3.8	2.8	–	–
$C_{lu}^{[aabb]}$	-0.03 ± 0.89	7.4	–	–
$C_{ld}^{[33aa]}$	-9.8 ± 5.3	–	–	–
$C_{ld}^{[aabb]}$	-0.4 ± 2.7	4.1	–	–
$C_{qe}^{[3333]}$	7.7 ± 7.4	–	–	–
$C_{qe}^{[aa33]}$	6.9 ± 4.4	2.6	–	–
$C_{qe}^{[33aa]}$	0.22 ± 0.38	10.0	–	–
$C_{qe}^{[aabb]}$	-0.23 ± 0.36	10.4	–	–
$C_{qu}^{(1)[3333]}$	0.3 ± 3.1	3.9	7.5 ± 7.5	–
$C_{qu}^{(1)[aa33]}$	0.1 ± 2.9	4.2	–	–
$C_{qu}^{(1)[33aa]}$	-7.0 ± 6.9	–	–	–
$C_{qu}^{(1)[aabb]}$	3.6 ± 9.1	–	–	–
$C_{qu}^{(8)[3333]}$	-10.3 ± 4.7	–	–	–
$C_{qu}^{(8)[aa33]}$	6.8 ± 6.1	–	–	–
$C_{qu}^{(8)[33aa]}$	-5.8 ± 8.2	–	–	–
$C_{quqd}^{(1)[3333]}$	-0.10 ± 0.40	10.2	–	–
$C_{quqd}^{(8)[3333]}$	-0.16 ± 0.48	9.2	–	–
$C_{lequ}^{(1)[3333]}$	-1.2 ± 3.7	3.5	–	–

References

- [1] A. Falkowski, *Lectures on SMEFT*, Eur. Phys. J. C **83** (2023), no. 7 656.
- [2] G. Isidori, F. Wilsch, and D. Wyler, *The standard model effective field theory at work*, Rev. Mod. Phys. **96** (2024), no. 1 015006, [[arXiv:2303.16922](#)].
- [3] J. Aebischer, A. J. Buras, and J. Kumar, *SMEFT ATLAS: The Landscape Beyond the Standard Model*, [[arXiv:2507.05926](#)].
- [4] J. de Blas, J. C. Criado, M. Perez-Victoria, and J. Santiago, *Effective description of general*

- extensions of the Standard Model: the complete tree-level dictionary*, JHEP **03** (2018) 109, [[arXiv:1711.10391](#)].
- [5] G. Guedes, P. Olgoso, and J. Santiago, *Towards the one loop IR/UV dictionary in the SMEFT: One loop generated operators from new scalars and fermions*, SciPost Phys. **15** (2023), no. 4 143, [[arXiv:2303.16965](#)].
- [6] G. Guedes and P. Olgoso, *From the EFT to the UV: the complete SMEFT one-loop dictionary*, [arXiv:2412.14253](#).
- [7] R. Aoude, T. Hurth, S. Renner, and W. Shepherd, *The impact of flavour data on global fits of the MFV SMEFT*, JHEP **12** (2020) 113, [[arXiv:2003.05432](#)].
- [8] D. A. Faroughy, G. Isidori, F. Wilsch, and K. Yamamoto, *Flavour symmetries in the SMEFT*, JHEP **08** (2020) 166, [[arXiv:2005.05366](#)].
- [9] S. Bißmann, C. Grunwald, G. Hiller, and K. Kröninger, *Top and Beauty synergies in SMEFT-fits at present and future colliders*, JHEP **06** (2021) 010, [[arXiv:2012.10456](#)].
- [10] S. Bruggisser, R. Schäfer, D. van Dyk, and S. Westhoff, *The Flavor of UV Physics*, JHEP **05** (2021) 257, [[arXiv:2101.07273](#)].
- [11] S. Bruggisser, D. van Dyk, and S. Westhoff, *Resolving the flavor structure in the MFV-SMEFT*, JHEP **02** (2023) 225, [[arXiv:2212.02532](#)].
- [12] L. Bellafronte, S. Dawson, and P. P. Giardino, *The importance of flavor in SMEFT Electroweak Precision Fits*, JHEP **05** (2023) 208, [[arXiv:2304.00029](#)].
- [13] C. Grunwald, G. Hiller, K. Kröninger, and L. Nollen, *More synergies from beauty, top, Z and Drell-Yan measurements in SMEFT*, JHEP **11** (2023) 110, [[arXiv:2304.12837](#)].
- [14] A. Greljo and A. Palavrić, *Leading directions in the SMEFT*, JHEP **09** (2023) 009, [[arXiv:2305.08898](#)].
- [15] L. Allwicher, C. Cornella, B. A. Stefanek, and G. Isidori, *New Physics in the Third Generation: A Comprehensive SMEFT Analysis and Future Prospects*, [arXiv:2311.00020](#).
- [16] R. Bartocci, A. Biekötter, and T. Hurth, *A global analysis of the SMEFT under the minimal MFV assumption*, JHEP **05** (2024) 074, [[arXiv:2311.04963](#)].
- [17] L. Mantani and V. Sanz, *Probing the flavour-blind SMEFT: EFT validity and the interplay of energy scales*, JHEP **06** (2025) 147, [[arXiv:2503.02935](#)].
- [18] S. Kala, L. Kolay, L. Mukherjee, and S. Nandi, *Constraining anomalous Wtb and related SMEFT couplings using low-energy and electroweak precision observables*, [arXiv:2505.07926](#).
- [19] E. Salvioni, G. Villadoro, and F. Zwirner, *Minimal Z-prime models: Present bounds and early LHC reach*, JHEP **11** (2009) 068, [[arXiv:0909.1320](#)].
- [20] R. Barbieri and G. Isidori, *Minimal flavour deconstruction*, JHEP **05** (2024) 033, [[arXiv:2312.14004](#)].
- [21] J. Ellis, M. Madigan, K. Mimasu, V. Sanz, and T. You, *Top, Higgs, Diboson and Electroweak Fit to the Standard Model Effective Field Theory*, JHEP **04** (2021) 279, [[arXiv:2012.02779](#)].
- [22] **SMEFiT** Collaboration, J. J. Ethier, G. Magni, F. Maltoni, L. Mantani, E. R. Nocera, J. Rojo, E. Slade, E. Vryonidou, and C. Zhang, *Combined SMEFT interpretation of Higgs, diboson, and top quark data from the LHC*, JHEP **11** (2021) 089, [[arXiv:2105.00006](#)].

- [23] F. Garosi, D. Marzocca, A. R. Sánchez, and A. Stanzione, *Indirect constraints on top quark operators from a global SMEFT analysis*, JHEP **12** (2023) 129, [[arXiv:2310.00047](#)].
- [24] E. Celada, T. Giani, J. ter Hoeve, L. Mantani, J. Rojo, A. N. Rossia, M. O. A. Thomas, and E. Vryonidou, *Mapping the SMEFT at high-energy colliders: from LEP and the (HL-)LHC to the FCC-ee*, JHEP **09** (2024) 091, [[arXiv:2404.12809](#)].
- [25] **ATLAS** Collaboration, G. Aad et al., *Interpretations of the ATLAS measurements of Higgs boson production and decay rates and differential cross-sections in pp collisions at $\sqrt{s} = 13$ TeV*, JHEP **11** (2024) 097, [[arXiv:2402.05742](#)].
- [26] R. Bartocci, A. Biekötter, and T. Hurth, *Renormalisation group evolution effects on global SMEFT analyses*, JHEP **05** (2025) 203, [[arXiv:2412.09674](#)].
- [27] **CMS** Collaboration, V. Chekhovsky et al., *Combined effective field theory interpretation of Higgs boson, electroweak vector boson, top quark, and multi-jet measurements*, .
- [28] J. ter Hoeve, L. Mantani, J. Rojo, A. N. Rossia, and E. Vryonidou, *Connecting scales: RGE effects in the SMEFT at the LHC and future colliders*, JHEP **06** (2025) 125, [[arXiv:2502.20453](#)].
- [29] E. E. Jenkins, A. V. Manohar, and P. Stoffer, *Low-Energy Effective Field Theory below the Electroweak Scale: Operators and Matching*, JHEP **03** (2018) 016, [[arXiv:1709.04486](#)]. [Erratum: JHEP 12, 043 (2023)].
- [30] J. de Blas et al., *HEPfit: a code for the combination of indirect and direct constraints on high energy physics models*, Eur. Phys. J. C **80** (2020), no. 5 456, [[arXiv:1910.14012](#)].
- [31] HEPfit Collaboration, <http://hepfit.roma1.infn.it>.
- [32] B. Grzadkowski, M. Iskrzynski, M. Misiak, and J. Rosiek, *Dimension-Six Terms in the Standard Model Lagrangian*, JHEP **10** (2010) 085, [[arXiv:1008.4884](#)].
- [33] **CMS** Collaboration, A. Tumasyan et al., *A portrait of the Higgs boson by the CMS experiment ten years after the discovery.*, Nature **607** (2022), no. 7917 60–68, [[arXiv:2207.00043](#)].
- [34] **ATLAS** Collaboration, G. Aad et al., *Combination of Searches for Higgs Boson Pair Production in pp Collisions at $s=13$ TeV with the ATLAS Detector*, Phys. Rev. Lett. **133** (2024), no. 10 101801, [[arXiv:2406.09971](#)].
- [35] L. Silvestrini and M. Valli, *Model-independent Bounds on the Standard Model Effective Theory from Flavour Physics*, Phys. Lett. B **799** (2019) 135062, [[arXiv:1812.10913](#)].
- [36] E. E. Jenkins, A. V. Manohar, and M. Trott, *Renormalization Group Evolution of the Standard Model Dimension Six Operators I: Formalism and lambda Dependence*, JHEP **10** (2013) 087, [[arXiv:1308.2627](#)].
- [37] E. E. Jenkins, A. V. Manohar, and M. Trott, *Renormalization Group Evolution of the Standard Model Dimension Six Operators II: Yukawa Dependence*, JHEP **01** (2014) 035, [[arXiv:1310.4838](#)].
- [38] R. Alonso, E. E. Jenkins, A. V. Manohar, and M. Trott, *Renormalization Group Evolution of the Standard Model Dimension Six Operators III: Gauge Coupling Dependence and Phenomenology*, JHEP **04** (2014) 159, [[arXiv:1312.2014](#)].
- [39] S. Descotes-Genon, A. Falkowski, M. Fedele, M. González-Alonso, and J. Virto, *The CKM parameters in the SMEFT*, JHEP **05** (2019) 172, [[arXiv:1812.08163](#)].

- [40] S. Di Noi and L. Silvestrini, *RGESolver: a C++ library to perform renormalization group evolution in the Standard Model Effective Theory*, Eur. Phys. J. C **83** (2023), no. 3 200, [[arXiv:2210.06838](#)].
- [41] A. Manohar and H. Georgi, *Chiral Quarks and the Nonrelativistic Quark Model*, Nucl. Phys. B **234** (1984) 189–212.
- [42] A. V. Manohar, *Introduction to Effective Field Theories*, [arXiv:1804.05863](#).
- [43] A. Caldwell, D. Kollar, and K. Kroninger, *BAT: The Bayesian Analysis Toolkit*, Comput. Phys. Commun. **180** (2009) 2197–2209, [[arXiv:0808.2552](#)].
- [44] L. Wolfenstein, *Parametrization of the Kobayashi-Maskawa Matrix*, Phys. Rev. Lett. **51** (1983) 1945.
- [45] L. Allwicher, D. A. Faroughy, F. Jaffredo, O. Sumensari, and F. Wilsch, *HighPT: A tool for high- p_T Drell-Yan tails beyond the standard model*, Comput. Phys. Commun. **289** (2023) 108749, [[arXiv:2207.10756](#)].
- [46] J. de Blas, M. Ciuchini, E. Franco, A. Goncalves, S. Mishima, M. Pierini, L. Reina, and L. Silvestrini, *Global analysis of electroweak data in the Standard Model*, Phys. Rev. D **106** (2022), no. 3 033003, [[arXiv:2112.07274](#)].
- [47] J. de Blas, M. Pierini, L. Reina, and L. Silvestrini, *Impact of the Recent Measurements of the Top-Quark and W-Boson Masses on Electroweak Precision Fits*, Phys. Rev. Lett. **129** (2022), no. 27 271801, [[arXiv:2204.04204](#)].
- [48] **CDF Collaboration**, T. Aaltonen et al., *High-precision measurement of the W boson mass with the CDF II detector*, Science **376** (2022), no. 6589 170–176.
- [49] **CMS Collaboration**, V. Chekhovsky et al., *High-precision measurement of the W boson mass with the CMS experiment at the LHC*, [arXiv:2412.13872](#).
- [50] **LHC-TeV MW Working Group Collaboration**, S. Amoroso et al., *Compatibility and combination of world W-boson mass measurements*, Eur. Phys. J. C **84** (2024), no. 5 451, [[arXiv:2308.09417](#)].
- [51] **Flavour Lattice Averaging Group (FLAG) Collaboration**, Y. Aoki et al., *FLAG Review 2021*, Eur. Phys. J. C **82** (2022), no. 10 869, [[arXiv:2111.09849](#)].
- [52] M. D. Brida, R. Höllwieser, F. Knechtli, T. Korzec, A. Ramos, S. Sint, and R. Sommer, *The strength of the interaction between quarks and gluons*, [arXiv:2501.06633](#).
- [53] **ALEPH, DELPHI, L3, OPAL, LEP Electroweak Collaboration**, S. Schael et al., *Electroweak Measurements in Electron-Positron Collisions at W-Boson-Pair Energies at LEP*, Phys. Rept. **532** (2013) 119–244, [[arXiv:1302.3415](#)].
- [54] **CMS Collaboration**, A. Tumasyan et al., *Precision measurement of the W boson decay branching fractions in proton-proton collisions at $\sqrt{s} = 13$ TeV*, Phys. Rev. D **105** (2022), no. 7 072008, [[arXiv:2201.07861](#)].
- [55] **D0 Collaboration**, B. Abbott et al., *A measurement of the W boson mass using electrons at large rapidities*, Phys. Rev. Lett. **84** (2000) 222–227, [[hep-ex/9909030](#)].
- [56] **CDF Collaboration**, A. Abulencia et al., *Measurements of inclusive W and Z cross sections in p anti-p collisions at $s^{*(1/2)} = 1.96$ -TeV*, J. Phys. G **34** (2007) 2457–2544, [[hep-ex/0508029](#)].

- [57] **D0** Collaboration, B. Abbott et al., *A measurement of the $W \rightarrow \tau\nu$ production cross section in $p\bar{p}$ collisions at $\sqrt{s} = 1.8$ TeV*, Phys. Rev. Lett. **84** (2000) 5710–5715, [[hep-ex/9912065](#)].
- [58] **CDF** Collaboration, F. Abe et al., *Measurement of the ratio $(W \rightarrow \tau\nu)/B(W \rightarrow e\nu)$, in $p\bar{p}$ collisions at $\sqrt{s} = 1.8$ TeV*, Phys. Rev. Lett. **68** (1992) 3398–3402.
- [59] **LHCb** Collaboration, R. Aaij et al., *Measurement of forward $W \rightarrow e\nu$ production in pp collisions at $\sqrt{s} = 8$ TeV*, JHEP **10** (2016) 030, [[arXiv:1608.01484](#)].
- [60] **ATLAS** Collaboration, M. Aaboud et al., *Precision measurement and interpretation of inclusive W^+ , W^- and Z/γ^* production cross sections with the ATLAS detector*, Eur. Phys. J. C **77** (2017), no. 6 367, [[arXiv:1612.03016](#)].
- [61] **ATLAS** Collaboration, G. Aad et al., *Test of the universality of τ and μ lepton couplings in W -boson decays with the ATLAS detector*, Nature Phys. **17** (2021), no. 7 813–818, [[arXiv:2007.14040](#)].
- [62] **LHCb** Collaboration, R. Aaij et al., *Measurement of $Z \rightarrow \tau^+\tau^-$ production in proton-proton collisions at $\sqrt{s} = 8$ TeV*, JHEP **09** (2018) 159, [[arXiv:1806.05008](#)].
- [63] L. Berthier, M. Bjørn, and M. Trott, *Incorporating doubly resonant W^\pm data in a global fit of SMEFT parameters to lift flat directions*, JHEP **09** (2016) 157, [[arXiv:1606.06693](#)].
- [64] **ATLAS, CMS** Collaboration, G. Aad et al., *Measurements of the Higgs boson production and decay rates and constraints on its couplings from a combined ATLAS and CMS analysis of the LHC pp collision data at $\sqrt{s} = 7$ and 8 TeV*, JHEP **08** (2016) 045, [[arXiv:1606.02266](#)].
- [65] **ATLAS** Collaboration, *Combined measurements of Higgs boson production and decay using up to 139 fb^{-1} of proton-proton collision data at $\sqrt{s} = 13$ TeV collected with the ATLAS experiment*, tech. rep., CERN, Geneva, 2021. All figures including auxiliary figures are available at <https://atlas.web.cern.ch/Atlas/GROUPS/PHYSICS/CONFNOTES/ATLAS-CONF-2021-053>.
- [66] **ATLAS** Collaboration, G. Aad et al., *A detailed map of Higgs boson interactions by the ATLAS experiment ten years after the discovery*, Nature **607** (2022), no. 7917 52–59, [[arXiv:2207.00092](#)]. [Erratum: Nature 612, E24 (2022)].
- [67] **ATLAS** Collaboration, G. Aad et al., *Characterising the Higgs boson with ATLAS data from the LHC Run-2*, Phys. Rept. **1116** (2025) 4–56, [[arXiv:2404.05498](#)].
- [68] **CMS** Collaboration, *Combined measurements and interpretations of Higgs boson production and decay at $\sqrt{s}=13$ TeV*, tech. rep., CERN, Geneva, 2025.
- [69] J. Alwall, R. Frederix, S. Frixione, V. Hirschi, F. Maltoni, O. Mattelaer, H. S. Shao, T. Stelzer, P. Torrielli, and M. Zaro, *The automated computation of tree-level and next-to-leading order differential cross sections, and their matching to parton shower simulations*, JHEP **07** (2014) 079, [[arXiv:1405.0301](#)].
- [70] I. Brivio, Y. Jiang, and M. Trott, *The SMEFTsim package, theory and tools*, JHEP **12** (2017) 070, [[arXiv:1709.06492](#)].
- [71] I. Brivio, *SMEFTsim 3.0 — a practical guide*, JHEP **04** (2021) 073, [[arXiv:2012.11343](#)].
- [72] A. Dedes, J. Rosiek, M. Ryczkowski, K. Suxho, and L. Trifyllis, *SmeftFR v3 – Feynman rules generator for the Standard Model Effective Field Theory*, Comput. Phys. Commun. **294** (2024) 108943, [[arXiv:2302.01353](#)].

- [73] C. Degrande, G. Durieux, F. Maltoni, K. Mimasu, E. Vryonidou, and C. Zhang, *Automated one-loop computations in the standard model effective field theory*, Phys. Rev. D **103** (2021), no. 9 096024, [[arXiv:2008.11743](#)].
- [74] M. Battaglia, M. Grazzini, M. Spira, and M. Wiesemann, *Sensitivity to BSM effects in the Higgs p_T spectrum within SMEFT*, JHEP **11** (2021) 173, [[arXiv:2109.02987](#)].
- [75] F. Maltoni, G. Ventura, and E. Vryonidou, *Impact of SMEFT renormalisation group running on Higgs production at the LHC*, JHEP **12** (2024) 183, [[arXiv:2406.06670](#)].
- [76] M. Czakon, P. Fiedler, and A. Mitov, *Resolving the Tevatron Top Quark Forward-Backward Asymmetry Puzzle: Fully Differential Next-to-Next-to-Leading-Order Calculation*, Phys. Rev. Lett. **115** (2015), no. 5 052001, [[arXiv:1411.3007](#)].
- [77] M. Czakon, P. Fiedler, D. Heymes, and A. Mitov, *NNLO QCD predictions for fully-differential top-quark pair production at the Tevatron*, JHEP **05** (2016) 034, [[arXiv:1601.05375](#)].
- [78] **CDF, D0** Collaboration, T. A. Aaltonen et al., *Combined Forward-Backward Asymmetry Measurements in Top-Antitop Quark Production at the Tevatron*, Phys. Rev. Lett. **120** (2018), no. 4 042001, [[arXiv:1709.04894](#)].
- [79] M. Czakon and A. Mitov, *Top++: A Program for the Calculation of the Top-Pair Cross-Section at Hadron Colliders*, Comput. Phys. Commun. **185** (2014) 2930, [[arXiv:1112.5675](#)].
- [80] M. Czakon, P. Fiedler, and A. Mitov, *Total Top-Quark Pair-Production Cross Section at Hadron Colliders Through $O(\alpha_S^4)$* , Phys. Rev. Lett. **110** (2013) 252004, [[arXiv:1303.6254](#)].
- [81] **ATLAS** Collaboration, G. Aad et al., *Measurement of the $t\bar{t}$ production cross-section and lepton differential distributions in $e\mu$ dilepton events from pp collisions at $\sqrt{s} = 13$ TeV with the ATLAS detector*, Eur. Phys. J. C **80** (2020), no. 6 528, [[arXiv:1910.08819](#)].
- [82] **ATLAS, CMS** Collaboration, G. Aad et al., *Combination of inclusive top-quark pair production cross-section measurements using ATLAS and CMS data at $\sqrt{s} = 7$ and 8 TeV*, JHEP **07** (2023) 213, [[arXiv:2205.13830](#)].
- [83] **ATLAS** Collaboration, G. Aad et al., *Measurement of the $t\bar{t}$ production cross-section in the lepton+jets channel at $\sqrt{s} = 13$ TeV with the ATLAS experiment*, Phys. Lett. B **810** (2020) 135797, [[arXiv:2006.13076](#)].
- [84] **ATLAS** Collaboration, G. Aad et al., *Measurements of top-quark pair differential and double-differential cross-sections in the ℓ +jets channel with pp collisions at $\sqrt{s} = 13$ TeV using the ATLAS detector*, Eur. Phys. J. C **79** (2019), no. 12 1028, [[arXiv:1908.07305](#)]. [Erratum: Eur.Phys.J.C 80, 1092 (2020)].
- [85] **CMS** Collaboration, A. M. Sirunyan et al., *Measurements of $t\bar{t}$ differential cross sections in proton-proton collisions at $\sqrt{s} = 13$ TeV using events containing two leptons*, JHEP **02** (2019) 149, [[arXiv:1811.06625](#)].
- [86] **CMS** Collaboration, A. Tumasyan et al., *Measurement of differential $t\bar{t}$ production cross sections in the full kinematic range using lepton+jets events from proton-proton collisions at $\sqrt{s} = 13$ TeV*, Phys. Rev. D **104** (2021), no. 9 092013, [[arXiv:2108.02803](#)].
- [87] **ATLAS** Collaboration, G. Aad et al., *Evidence for the charge asymmetry in $pp \rightarrow t\bar{t}$ production at $\sqrt{s} = 13$ TeV with the ATLAS detector*, JHEP **08** (2023) 077, [[arXiv:2208.12095](#)].

- [88] A. Broggio, A. Ferroglia, R. Frederix, D. Pagani, B. D. Pecjak, and I. Tsinikos, *Top-quark pair hadroproduction in association with a heavy boson at NLO+NNLL including EW corrections*, JHEP **08** (2019) 039, [[arXiv:1907.04343](#)].
- [89] CMS Collaboration, A. M. Sirunyan et al., *Measurement of top quark pair production in association with a Z boson in proton-proton collisions at $\sqrt{s} = 13$ TeV*, JHEP **03** (2020) 056, [[arXiv:1907.11270](#)].
- [90] ATLAS Collaboration, G. Aad et al., *Inclusive and differential cross-section measurements of $t\bar{t}Z$ production in pp collisions at $\sqrt{s} = 13$ TeV with the ATLAS detector, including EFT and spin-correlation interpretations*, JHEP **07** (2024) 163, [[arXiv:2312.04450](#)].
- [91] G. Bevilacqua, H. Hartanto, M. Kraus, T. Weber, and M. Worek, *Hard Photons in Hadroproduction of Top Quarks with Realistic Final States*, JHEP **10** (2018) 158, [[arXiv:1803.09916](#)].
- [92] G. Bevilacqua, H. Hartanto, M. Kraus, T. Weber, and M. Worek, *Precise predictions for $t\bar{t}\gamma/t\bar{t}$ cross section ratios at the LHC*, JHEP **01** (2019) 188, [[arXiv:1809.08562](#)].
- [93] CMS Collaboration, A. Tumasyan et al., *Measurement of the inclusive and differential $t\bar{t}\gamma$ cross sections in the single-lepton channel and EFT interpretation at $\sqrt{s} = 13$ TeV*, JHEP **12** (2021) 180, [[arXiv:2107.01508](#)].
- [94] CMS Collaboration, A. Tumasyan et al., *Measurement of the inclusive and differential $t\bar{t}\gamma$ cross sections in the dilepton channel and effective field theory interpretation in proton-proton collisions at $\sqrt{s} = 13$ TeV*, JHEP **05** (2022) 091, [[arXiv:2201.07301](#)].
- [95] ATLAS Collaboration, G. Aad et al., *Measurements of inclusive and differential cross-sections of combined $t\bar{t}\gamma$ and $tW\gamma$ production in the $e\mu$ channel at 13 TeV with the ATLAS detector*, JHEP **09** (2020) 049, [[arXiv:2007.06946](#)].
- [96] R. Frederix, D. Pagani, and M. Zaro, *Large NLO corrections in $t\bar{t}W^\pm$ and $t\bar{t}\bar{t}$ hadroproduction from supposedly subleading EW contributions*, JHEP **02** (2018) 031, [[arXiv:1711.02116](#)].
- [97] L. Buonocore, S. Devoto, M. Grazzini, S. Kallweit, J. Mazzitelli, L. Rottoli, and C. Savoini, *Precise Predictions for the Associated Production of a W Boson with a Top-Antitop Quark Pair at the LHC*, Phys. Rev. Lett. **131** (2023), no. 23 231901, [[arXiv:2306.16311](#)].
- [98] ATLAS Collaboration, G. Aad et al., *Measurement of the total and differential cross-sections of $t\bar{t}W$ production in pp collisions at $\sqrt{s} = 13$ TeV with the ATLAS detector*, JHEP **05** (2024) 131, [[arXiv:2401.05299](#)].
- [99] CMS Collaboration, A. Tumasyan et al., *Measurement of the cross section of top quark-antiquark pair production in association with a W boson in proton-proton collisions at $\sqrt{s} = 13$ TeV*, JHEP **07** (2023) 219, [[arXiv:2208.06485](#)].
- [100] A. Czarnecki, J. G. Körner, and J. H. Piclum, *Helicity fractions of w bosons from top quark decays at next-to-next-to-leading order in qcd*, Phys. Rev. D **81** (Jun, 2010) 111503.
- [101] ATLAS and CMS Collaborations, *Combination of the W boson polarization measurements in top quark decays using ATLAS and CMS data at $\sqrt{s} = 8$ TeV*, JHEP **08** (2020), no. 08 051, [[arXiv:2005.03799](#)].
- [102] ATLAS Collaboration, G. Aad et al., *Measurement of the polarisation of W bosons produced in top-quark decays using dilepton events at $s=13$ TeV with the ATLAS experiment*, Phys. Lett. B **843** (2023) 137829, [[arXiv:2209.14903](#)].

- [103] N. Kidonakis, *Two-loop soft anomalous dimensions for single top quark associated production with a W^- or H^-* , Phys. Rev. D **82** (2010) 054018, [[arXiv:1005.4451](#)].
- [104] **ATLAS, CMS** Collaboration, M. Aaboud et al., *Combinations of single-top-quark production cross-section measurements and $-f_{LV} V_{tb}$ determinations at $\sqrt{s} = 7$ and 8 TeV with the ATLAS and CMS experiments*, JHEP **05** (2019) 088, [[arXiv:1902.07158](#)].
- [105] **ATLAS** Collaboration, M. Aaboud et al., *Measurement of the cross-section for producing a W boson in association with a single top quark in pp collisions at $\sqrt{s} = 13$ TeV with ATLAS*, JHEP **01** (2018) 063, [[arXiv:1612.07231](#)].
- [106] **CMS** Collaboration, A. Tumasyan et al., *Measurement of inclusive and differential cross sections for single top quark production in association with a W boson in proton-proton collisions at $\sqrt{s} = 13$ TeV*, JHEP **07** (2023) 046, [[arXiv:2208.00924](#)].
- [107] M. Aliev, H. Lacker, U. Langenfeld, S. Moch, P. Uwer, and M. Wiedermann, *HATHOR: HAdronic Top and Heavy quarks crOss section calculatoR*, Comput. Phys. Commun. **182** (2011) 1034–1046, [[arXiv:1007.1327](#)].
- [108] P. Kant, O. Kind, T. Kintscher, T. Lohse, T. Martini, S. Mölbitz, P. Rieck, and P. Uwer, *HatHor for single top-quark production: Updated predictions and uncertainty estimates for single top-quark production in hadronic collisions*, Comput. Phys. Commun. **191** (2015) 74–89, [[arXiv:1406.4403](#)].
- [109] D. Muller, Search for single top quark production in the s channel at 13 TeV with the CMS experiment. PhD thesis, Karlsruhe Institute for Technology, 2020. Presented 05 Jun 2020.
- [110] **ATLAS** Collaboration, G. Aad et al., *Measurement of single top-quark production in the s-channel in proton–proton collisions at $\sqrt{s} = 13$ TeV with the ATLAS detector*, JHEP **06** (2023) 191, [[arXiv:2209.08990](#)].
- [111] **CMS** Collaboration, A. M. Sirunyan et al., *Measurement of the single top quark and antiquark production cross sections in the t channel and their ratio in proton-proton collisions at $\sqrt{s} = 13$ TeV*, Phys. Lett. B **800** (2020) 135042, [[arXiv:1812.10514](#)].
- [112] **ATLAS** Collaboration, G. Aad et al., *Measurement of t-channel production of single top quarks and antiquarks in pp collisions at 13 TeV using the full ATLAS Run 2 data sample*, JHEP **05** (2024) 305, [[arXiv:2403.02126](#)].
- [113] **ATLAS** Collaboration, G. Aad et al., *Observation of Single-Top-Quark Production in Association with a Photon Using the ATLAS Detector*, Phys. Rev. Lett. **131** (2023), no. 18 181901, [[arXiv:2302.01283](#)].
- [114] **CMS** Collaboration, A. M. Sirunyan et al., *Evidence for the associated production of a single top quark and a photon in proton-proton collisions at $\sqrt{s} = 13$ TeV*, Phys. Rev. Lett. **121** (2018), no. 22 221802, [[arXiv:1808.02913](#)].
- [115] **CMS** Collaboration, A. Tumasyan et al., *Inclusive and differential cross section measurements of single top quark production in association with a Z boson in proton-proton collisions at $\sqrt{s} = 13$ TeV*, JHEP **02** (2022) 107, [[arXiv:2111.02860](#)].
- [116] **ATLAS** Collaboration, G. Aad et al., *Observation of the associated production of a top quark and a Z boson in pp collisions at $\sqrt{s} = 13$ TeV with the ATLAS detector*, JHEP **07** (2020) 124, [[arXiv:2002.07546](#)].

- [117] **CMS** Collaboration, A. M. Sirunyan et al., *Measurement of the cross section for $t\bar{t}$ production with additional jets and b jets in pp collisions at $\sqrt{s} = 13$ TeV*, JHEP **07** (2020) 125, [[arXiv:2003.06467](#)].
- [118] M. van Beekveld, A. Kulesza, and L. M. Valero, *Threshold Resummation for the Production of Four Top Quarks at the LHC*, Phys. Rev. Lett. **131** (2023), no. 21 211901, [[arXiv:2212.03259](#)].
- [119] **ATLAS** Collaboration, G. Aad et al., *Measurement of the $t\bar{t}\bar{t}$ production cross section in pp collisions at $\sqrt{s} = 13$ TeV with the ATLAS detector*, JHEP **11** (2021) 118, [[arXiv:2106.11683](#)].
- [120] **CMS** Collaboration, A. Hayrapetyan et al., *Observation of four top quark production in proton-proton collisions at $s=13$ TeV*, Phys. Lett. B **847** (2023) 138290, [[arXiv:2305.13439](#)].
- [121] **ATLAS** Collaboration, G. Aad et al., *Observation of four-top-quark production in the multilepton final state with the ATLAS detector*, Eur. Phys. J. C **83** (2023), no. 6 496, [[arXiv:2303.15061](#)]. [Erratum: Eur.Phys.J.C 84, 156 (2024)].
- [122] G. Durieux, A. Irlles, V. Miralles, A. Peñuelas, R. Pöschl, M. Perelló, and M. Vos, *The electro-weak couplings of the top and bottom quarks — Global fit and future prospects*, JHEP **12** (2019) 98, [[arXiv:1907.10619](#)]. [Erratum: JHEP 01, 195 (2021)].
- [123] V. Miralles, M. Miralles López, M. Moreno Llácer, A. Peñuelas, M. Perelló, and M. Vos, *The top quark electro-weak couplings after LHC Run 2*, JHEP **02** (2022) 032, [[arXiv:2107.13917](#)].
- [124] F. Cornet-Gomez, V. Miralles, M. Miralles López, M. Moreno Llácer, and M. Vos, *Future collider constraints on top-quark operators*, [arXiv:2503.11518](#).
- [125] M. Czakon, D. Heymes, and A. Mitov, *Dynamical scales for multi-TeV top-pair production at the LHC*, JHEP **04** (2017) 071, [[arXiv:1606.03350](#)].
- [126] E. E. Jenkins, A. V. Manohar, and P. Stoffer, *Low-Energy Effective Field Theory below the Electroweak Scale: Anomalous Dimensions*, JHEP **01** (2018) 084, [[arXiv:1711.05270](#)]. [Erratum: JHEP 12, 042 (2023)].
- [127] **Particle Data Group** Collaboration, S. Navas et al., *Review of particle physics*, Phys. Rev. D **110** (2024), no. 3 030001.
- [128] M. Ciuchini, E. Franco, V. Lubicz, G. Martinelli, L. Silvestrini, and C. Tarantino, *Power corrections to the CP-violation parameter ε_K* , JHEP **02** (2022) 181, [[arXiv:2111.05153](#)].
- [129] B. Wang, *Calculating Δm_K with lattice QCD*, PoS LATTICE2021 (2022) 141, [[arXiv:2301.01387](#)].
- [130] F. Betti et al., *Global analysis of charm mixing parameters and determination of the CKM angle γ* , [arXiv:2409.06449](#).
- [131] M. Di Carlo, D. Giusti, V. Lubicz, G. Martinelli, C. T. Sachrajda, F. Sanfilippo, S. Simula, and N. Tantalo, *Light-meson leptonic decay rates in lattice QCD+QED*, Phys. Rev. D **100** (2019), no. 3 034514, [[arXiv:1904.08731](#)].
- [132] G. Isidori, F. Mescia, and C. Smith, *Light-quark loops in $K \rightarrow \pi \nu \text{ anti-}\nu$* , Nucl. Phys. B **718** (2005) 319–338, [[hep-ph/0503107](#)].

- [133] **HFLAV** Collaboration, Y. S. Amhis et al., *Averages of b -hadron, c -hadron, and τ -lepton properties as of 2021*, Phys. Rev. D **107** (2023), no. 5 052008, [[arXiv:2206.07501](#)].
- [134] M. Ciuchini, M. Pierini, and L. Silvestrini, *The Effect of penguins in the $B_d \rightarrow J/\psi K0$ CP asymmetry*, Phys. Rev. Lett. **95** (2005) 221804, [[hep-ph/0507290](#)].
- [135] **Belle** Collaboration, R. Glattauer et al., *Measurement of the decay $B \rightarrow D\ell\nu_\ell$ in fully reconstructed events and determination of the Cabibbo-Kobayashi-Maskawa matrix element $|V_{cb}|$* , Phys. Rev. D **93** (2016), no. 3 032006, [[arXiv:1510.03657](#)].
- [136] **UTfit** Collaboration, M. Bona et al., *New UTfit Analysis of the Unitarity Triangle in the Cabibbo-Kobayashi-Maskawa scheme*, Rend. Lincei Sci. Fis. Nat. **34** (2023) 37–57, [[arXiv:2212.03894](#)].
- [137] M. Bona et al., *Overview and theoretical prospects for CKM matrix and CP violation from the UTfit Collaboration*, PoS WIFAI2023 (2024) 007.
- [138] F. Gabbiani, E. Gabrielli, A. Masiero, and L. Silvestrini, *A Complete analysis of FCNC and CP constraints in general SUSY extensions of the standard model*, Nucl. Phys. B **477** (1996) 321–352, [[hep-ph/9604387](#)].
- [139] **UTfit** Collaboration, M. Bona et al., *Constraints on new physics from the quark mixing unitarity triangle*, Phys. Rev. Lett. **97** (2006) 151803, [[hep-ph/0605213](#)].
- [140] **UTfit** Collaboration, M. Bona et al., *Model-independent constraints on $\Delta F = 2$ operators and the scale of new physics*, JHEP **03** (2008) 049, [[arXiv:0707.0636](#)].
- [141] **MILC** Collaboration, J. A. Bailey et al., *$B \rightarrow D\ell\nu$ form factors at nonzero recoil and $-V_{cb}$ from 2+1-flavor lattice QCD*, Phys. Rev. D **92** (2015), no. 3 034506, [[arXiv:1503.07237](#)].
- [142] M. Misiak, A. Rehman, and M. Steinhauser, *Towards $\bar{B} \rightarrow X_s\gamma$ at the NNLO in QCD without interpolation in m_c* , JHEP **06** (2020) 175, [[arXiv:2002.01548](#)].
- [143] C. Bobeth, M. Gorbahn, T. Hermann, M. Misiak, E. Stamou, and M. Steinhauser, *$B_{s,d} \rightarrow l^+l^-$ in the Standard Model with Reduced Theoretical Uncertainty*, Phys. Rev. Lett. **112** (2014) 101801, [[arXiv:1311.0903](#)].
- [144] J. Brod, M. Gorbahn, and E. Stamou, *Two-Loop Electroweak Corrections for the $K \rightarrow \pi\nu\bar{\nu}$ Decays*, Phys. Rev. D **83** (2011) 034030, [[arXiv:1009.0947](#)].
- [145] J. Brod, M. Gorbahn, and E. Stamou, *Updated Standard Model Prediction for $K \rightarrow \pi\nu\bar{\nu}$ and ϵ_K* , PoS BEAUTY2020 (2021) 056, [[arXiv:2105.02868](#)].
- [146] F. Krauss, S. Kuttimalai, and T. Plehn, *LHC multijet events as a probe for anomalous dimension-six gluon interactions*, Phys. Rev. D **95** (2017), no. 3 035024, [[arXiv:1611.00767](#)].
- [147] V. Hirschi, F. Maltoni, I. Tsirikos, and E. Vryonidou, *Constraining anomalous gluon self-interactions at the LHC: a reappraisal*, JHEP **07** (2018) 093, [[arXiv:1806.04696](#)].
- [148] A. Falkowski and F. Riva, *Model-independent precision constraints on dimension-6 operators*, JHEP **02** (2015) 039, [[arXiv:1411.0669](#)].
- [149] J. de Blas, M. Chala, and J. Santiago, *Renormalization Group Constraints on New Top Interactions from Electroweak Precision Data*, JHEP **09** (2015) 189, [[arXiv:1507.00757](#)].
- [150] B. A. Stefanek, *Non-universal probes of composite Higgs models: new bounds and prospects for FCC-ee*, JHEP **09** (2024) 103, [[arXiv:2407.09593](#)].